Generation and characterization of novel co-stimulatory anti-mouse TNFR2 antibodies

Generation and characterization of novel co-stimulatory anti-mouse TNFR2 antibodies

Authors

Aina Segués[a,b,c], Sander M.J. van Duijnhoven[a], Marc Parade[a], Lilian Driessen[a], Nataša Vukovic[d], Dietmar Zaiss[d,e], Alice J. A. M. Sijts[b], Pedro Berraondo[d], Andrea van Elsas[a,*]

Affiliation

[a] *Aduro Biotech Europe, Oss, The Netherlands*

[b] *Faculty of Veterinary Medicine, Department of Infectious Diseases and Immunology, Utrecht University, Utrecht, The Netherlands*

[c] *Division of Immunology and Immunotherapy, Cima Universidad de Navarra, Pamplona, Spain*

[d] *Institute of Immunology and Infection Research, School of Biological Sciences, University of Edinburgh, United Kingdom*

[e] *Institute of Immune Medicine, University Hospital Regensburg, Regensburg, Germany.*

* Corresponding author

E-mail address: andrea.vanelsas@gmail.com

Abstract

Tumor necrosis factor receptor 2 (TNFR2) has gained much research interest in recent years because of its potential pivotal role in autoimmune disease and cancer. However, its function in regulating different immune cells is not well understood. There is a need for well-characterized reagents to selectively modulate TNFR2 function, thereby enabling definition of TNFR2-dependent biology in human and mouse surrogate models. Here, we describe the generation, production, purification, and characterization of a panel of novel antibodies targeting mouse TNFR2. The antibodies display functional differences in binding affinity and potency to block TNFα. Furthermore, epitope binding showed that the anti-mTNFR2 antibodies target different domains on the TNFR2 protein, associated with varying capacity to enhance $CD8^+$ T-cell activation and costimulation. Moreover, the anti-TNFR2 antibodies demonstrate binding to isolated splenic mouse Tregs *ex vivo* and activated CD8+ cells, reinforcing their potential use to establish TNFR2-dependent immune modulation in translational models of autoimmunity and cancer.

Key words

TNFR2, antibody, epitope, Cysteine-Rich Domain, costimulation, Treg

Highlights

- We have generated a diverse library of anti-mouse TNFR2 antibodies
- Developed anti-mouse TNFR2 antibodies show binding to regulatory T cells (Tregs) and activated CD8+ cells
- Some anti-mouse TNFR2 antibodies costimulate CD8+ cells

1. Introduction

The immune system encodes multiple controls evolved to ensure a balance of immune homeostasis ready to fight infections and inhibit the development of cancer, but also aiming to prevent unwanted inflammation and autoimmunity. A disbalance in immune regulation can contribute to immune overreaction, as recently observed in severe Covid-19 cases[1], leading to autoimmune and infectious disease, inadequate tumor immunity, or even immune paralysis in sepsis. Blockade of immune checkpoint receptors such as programmed cell death protein 1 (PD-1) and cytotoxic T lymphocyte-associated protein 4 (CTLA-4) plays an important role in the treatment of cancer [2,3]. In contrast, defects in or deliberate blockade of immune checkpoint pathways may result in the loss of peripheral tolerance and autoimmunity[4]. Enhancing the activity of immune checkpoint pathways potentially using agonistic agents may hold promise for the treatment of autoimmunity [5,6]. In this context, tumor necrosis factor receptor 2 (TNFR2; TNFRSF1B; CD120b) might act as an immune checkpoint on T lymphocytes.

In the past decade, the interest to target the co-stimulatory tumor necrosis factor receptor superfamily (TNFRSF) for immunotherapy of cancer[7,8] and autoimmune disease[9,10] has increased significantly. Approximately 30 members of the TNFRSF have been identified. TNFRSF, together with its respective ligands, control cell survival, proliferation, differentiation, and effector function in different cell types, including immune cells[11]. Some of these receptors have already been defined to play a crucial role in immune dysfunction, autoimmunity, and cancer. For example, the CD40L-CD40 interaction has been shown to be correlated with inflammatory and muscle wasting diseases[12,13]. Furthermore, promotion of antitumor T cell activity has been achieved by using several agonistic anti-CD40 antibodies[14,15], and other examples include antibodies targeting CD27, 4-1BB, and OX40. However, these agonists are not yet a clinical success, likely due to promiscuous expression and function on other cells leading to safety concerns.

Tumor necrosis factor α (TNFα) is involved in several immune response pathways mediating its activity via TNF receptor 1 (TNFR1) and TNF receptor 2 (TNFR2). While TNFR1 is ubiquitously expressed on almost all cell types[16], TNFR2 expression is limited to certain subpopulations of immune cells. Beyond its expression on specific immune cell subpopulations, TNFR2 expression has also been described for several other cell types, such as oligodendrocytes, cardiomyocytes, mesenchymal stem cells and endothelial progenitor cell [17–20]. TNFα is the principal ligand of TNFR1 and TNFR2. TNFR1 receptor signaling is activated through both soluble and membrane TNF-α, whereas TNFR2 is mainly activated by membrane TNF-α[21]. However, while TNFR1 stimulation can trigger both a strong pro-inflammatory response as well as cell death through its death domains, TNFR2 stimulation has so far only be involved in cell survival, proliferation and differentiation as well as inducing a more anti-inflammatory response[22].

Due to its inducible expression on regulatory T cells (Tregs), TNFR2 has been identified as an important target in autoimmune diseases and cancer[23]. In mice, the highest TNFR2 expression is found on Tregs with potent immunosuppressive capacity, as well as on conventional T cells that resist Treg mediated immunosuppression. However, overall, in tumor-derived T cell populations, the suppressive effect appears to be dominant[24]. In cancer cells, TNFR2 expression has been correlated with tumor growth[25] and its absence in $CD8^+$ T cells with enhanced immune rejection[26]. TNFR2 signaling in innate immune lymphocytes enhanced allergic lung inflammation[27]. However, consistent with a role in Tregs, TNFR2 signaling suppressed autoimmunity in the central nervous system[28]. Furthermore, the induction of Treg differentiation by specific cell types, such as mesenchymal stem cells, has also been shown to be TNFR2 dependent[29]. Therefore, TNFR2 is an appealing target in both cancer and autoimmune disease. Although TNFR2 was recently considered an immune checkpoint, its role

in different immune cells and diseases is not well understood and requires well-defined reagents.

Here, we generated and characterized the activity of a novel panel of 13 diverse rat anti-mouse TNFR2 antibodies. The panel contains antibodies that bind to different extracellular domains of TNFR2 and selectively display varying functional capacity. These novel antibodies have been sequenced and classified based on their binding and blocking activity, epitope binning with respect to binding of specific TNFR2 extracellular domains, and their capacity to enhance costimulation of $CD8^+$ T-cell activation. Furthermore, a subset of antibodies demonstrates potent binding to TNFR2 on the surface of mouse Tregs and activated C8+ cells. This diverse set of well-characterized antibodies may serve to explore further TNFR2 function in mouse models of health and disease.

2. Material and methods

2.1 Cell lines

All cell lines were maintained at 37 °C in a humidified 5% CO_2 incubator. CHO-K1 cells were cultured in DMEM/F12 (Gibco, 11320-074) supplemented with 100 U/mL Penicillin, 100 µg/mL Streptomycin (Gibco, 15140-122), and 5% NBCS (Biowest, S0750-500). Additionally, 0.8 mg/mL Geneticin (Gibco, 19131-027) was added to stable transfected CHO-K1.mTNFR2. B-cells were cultured in DMEM/F12 HAM medium (Sigma Aldrich, D6421) supplemented with 365 mg/L L-glutamine (Gibco, 25030), 0.5 mM Sodium pyruvate (Gibco, 11360-039), 50 µM 2-mercaptoethanol (Gibco, 31350-010), 100 U/mL Penicillin, 100 µg/mL Streptomycin (Gibco, 15140-122), and 10% BCS (Hyclone, SH30072.03) in the presence of 5 x 10^5 cells/mL irradiated EL.4 B5 cells (feeder cells). SP2/0-Ag14 cells were cultured in DMEM/F12 (Gibco, 11320-074) supplemented with 100 U/mL Penicillin, 100 µg/mL Streptomycin (Gibco, 15140-122), 50 µM 2-mercaptoethanol (Gibco, 31350-010), and 10% FBS (Hyclone, SH30414.02).

Hybridomas were selected in DMEM/F12 medium (Gibco, 11320-074) supplemented with 0.5 mM Sodium pyruvate (Gibco, 11360-039), 50 μM 2-mercaptoethanol (Gibco, 31350-010), 100 U/mL Penicillin, 100 μg/mL Streptomycin (Gibco, 15140-122), 10% FBS (Hyclone, SH30414.02), 1% T24 conditioned media, and 2% HAT supplement 50X (Gibco, 21060-017). Hybridomas were cultured in DMEM/F12 medium (Gibco, 11320-074) supplemented with 0.5 mM Sodium pyruvate (Gibco, 11360-039), 50 μM 2-mercaptoethanol (Gibco, 31350-010), 100 U/mL Penicillin, 100 μg/mL Streptomycin (Gibco, 15140-122), 10% NBCS (Biowest, S0750-500), 1% T24CM, and 1% HT supplement 100X (Gibco, 11067-030).

2.2 Generation of hybridomas producing monoclonal antibodies (mAbs)

Three 9-week-old female Spraque Dawley rats were immunized on the ears using mTNFR2 encoding DNA coated gold-carrier beads via gene gun. After 4 rounds of immunization, cells derived from lymph nodes, spleen, and bone marrow were harvested and TNFR2 specific B cells isolated following published procedures[30]. Briefly, negative and positive panning strategies were performed to select TNFR2 specific B-cells. Culture plates with CHO-K1 and transiently transfected CHO-K1 with mouse TNFR1, or in parallel plates coated with mIgG and mTNFR1 recombinant protein were used for negative panning as cross-reactivity to mTNFR1 was non desired. TNFR2 expressed on cells or recombinant mTNFR2 protein were used for positive panning.

CHO-K1.mTNFR2 or mTNFR2 protein-bound lymphocytes were harvested with Trypsin-EDTA (Sigma Aldrich, T4174). Harvested B-cells were cultured, as described by Steenbakkers et al., 1994, Mol. Biol. Rep. 19: 125-134[31]. Briefly, selected B-cells were mixed with 10% (v/v) T-cell supernatant and 50,000 irradiated (25 Gray) EL-4 B5 feeder cells in a final volume of 200 μL medium in 96-well flat-bottom tissue culture plates and were cultured at 37°C and 95% humidity for 9 days.

Immunoreactivity to mouse TNFR2 and cross-reactivity to human TNFR2 was assessed by ELISA using recombinant mTNFR2/Fc-protein (R&D Systems, 9707-R2) and hTNFR2 (R&D Systems, 726-R2) as well as CHO-K1.mTNFR2 and CHO-K1.hTNFR2. 0.1µg/ml mTNFR2 and 0.2µg/ml hTNFR2 protein-coated 96-well plates were blocked in PBS/1% bovine serum albumin (BSA) (Sigma Aldrich, A7409) for 1 hour at room temperature (RT). Assay plates with B-cell conditioned medium were incubated for 1 hour at RT. Next, plates were washed with PBS-T and incubated for 1 hour at RT with goat-anti-rat IgG-HRP conjugate (Jackson Immuno Research, 112-035-167). Subsequently, wells were washed three times with PBS-T, and anti-mTNFR2 immunoreactivity was visualized with TMB Stabilized Chromogen (Invitrogen, SB02). Reactions were stopped with 0.5 M H_2SO_4, and absorbances were read at 420 and 620 nm.

B-cell clones that showed specific binding to mTNFR2 (with or without cross-reactivity toward hTNFR2) and no cross-reactivity to TNFR1 were immortalized by mini-electrofusion following published procedures (Steenbakkers et al., 1992, J. Immunol. Meth. 152: 69-77; Steenbakkers et al., 1994, Mol. Biol. Rep. 19:125-34)[31,32] with some minor deviations.

Briefly, B-cells were mixed with $1x10^6$ Sp2/0-Ag14 murine myeloma cells in Electrofusion Isomolar Buffer (Eppendorf). Electrofusions were performed in a 50 µL fusion chamber by an alternating electric field of 15 s, 1 MHz, 23 Vrms AC followed by a square, high field DC pulse of 10 µs, 180 Volt DC and again by an alternating electric field of 15 s, 1 MHz, 23 Vrms AC. Content of the chamber was transferred to hybridoma selective medium and plated in a 96-well plate under limiting dilution conditions. On day 10 following the electrofusion, hybridoma supernatants were screened for mTNFR2, hTNFR2, mTNFR1 binding activity by and ELISA, as described above. Hybridomas that secreted antibodies in the supernatant that specifically

bound mTNFR2 and/or hTNFR2 were both frozen at -180°C and subcloned by limited dilution to safeguard their clonal integrity and stability.

28 hybridomas clones producing different anti-mTNR2 were obtained, and based on different characteristics, 13 candidates were selected to be further characterized, methods, and results shown in this manuscript. Generated antibodies were sent for sequencing, and sequences can be found attached in Sup. Table 1. All antibodies were tested for their isotype using the Rat Monoclonal Antibody Isotyping Test Kit (Bio-Rad, RMT1) following manufacturer's instructions.

2.3 Production and purification of mAbs

13 hybridomas clones producing different anti-mTNFR2 antibodies were incubated in hybridoma serum-free medium (HSFM) (Gibco, 12045-076) supplemented with serum-free T24 CM and 100 U/mL Penicillin and 100 µg/mL Streptomycin (Gibco, 15140-122) at a density of 5 x 10^5 cells/mL for 7 days at 37 °C in 8% CO_2 at 80 rpm. Cells were spun down, and the supernatant was filtered through a 0.22 µm filter. All anti-mTNFR2 mAbs were purified by GammaBind Plus Sepharose (GE Healthcare, 17-0886-01) followed by size exclusion chromatography (SEC) using a Waters BEH200 SEC column (4.6 x 300 mm, 1.7µm). mAbs were rebuffered in 10mM L-Histidine 0.1M NaCl pH 5.5.

2.4 Quality control

Monomericity of mAbs was tested via Size Exclusion Chromatography Ultra Performance Liquid Chromatography (SEC-UPLC) on a Waters BEH200 SEC column, 4.6 x 300 mm, 1.7 µm with an Agilent 1100 series HPLC system. Separation was carried out in 50mM phosphate 0.2M NaCl, pH 7.0. The monomericity was also tested following incubation and storage at different temperatures to assess protein stability. Two temperature studies were performed: (i) 10 freeze and thaw (F/T) cycles and (ii) incubation at 40 °C for one

week. Based on the initial monomericity, the stability has been reported as the recovery percentage.

The purity of mAbs produced was tested by Capillary electrophoresis sodium dodecyl sulfate (CE-SDS) in non-reduced mode. CE-SDS analysis was carried out on a CE system PA800 Plus machine (Beckman Coulter). Non-reduced samples were diluted to 1 mg/mL with 10kDa internal standard and 15mM iodoacetamide in SDS-MW sample buffer and heated to 70 °C for 10 min. Reduced samples were diluted to 1 mg/mL with 10kDa internal standard and 2-mercaptoethanol (Sigma Aldrich, M3148) in SDS-MW sample buffer and heated to 70 °C for 10 min. 95 µL were transferred into sample vials and loaded into the machine. Separations were performed in a 30 cm bara-fused silica 50 µm I.D capillary at 22 °C. The capillary was flushed with 0.1 M HCl, NaOH, water, and running buffer before sample loading at 5kV for 20sec. Data acquisition was performed with the 32Karat software, but data processing was carried out with Empower software.

2.5 Flow cytometry: Cell binding and TNFα blocking assay

Binding potency of the anti-mTNFR2 mAbs on mTNFR2 CHO-K1 stable transfected cell line was assessed by flow cytometry. 1 x 10^5 cells were incubated with 3-fold increasing concentrations (max 10 µg/mL) of anti-mTNFR2 mAbs at 4 °C for 30 min, and binding was detected with anti-rat IgG PE (BD Biosciences, 550767). TNFR2 expression of the cell line was assessed via hamster anti-mouse CD120b (TNF R Type II/p75) -PE (TR75-89) (Biolegend, 113405), and hamster IgG1 isotype control-PE (BD Biosciencies, 553972) was used as a negative control.

For all anti-mTNFR2 mAbs, competitive binding in the presence of TNFα was assessed with CHO-K1.mTNFR2 stable transfected cell line by flow cytometry. 1 x 10^5 cells were incubated with 3-fold increasing concentrations (max 50 µg/mL) of anti-mTNFR2 mAbs at 4 °C for 30

min followed by TNFα-biotin (Sino Biological, 50349-MNAE-B) incubation at 4 °C for 30 min without wash step. Blocking activity was detected with Streptavidin-APC (BD Biosciences, 349024). Two benchmark hamster antibodies against mTNFR2 were taken as a reference: Purified anti-mouse CD120b (TNFR Type II/p75, clone TR75-54.7) (Biolegend, 113302) listed as anti-TNFR2 mAb with blocking activity and Purified anti-mouse CD120b (TNFR Type II/p75, clone TR75-89) (BD Biosciencies, 559916) as a non-blocking anti-TNFR2 mAb. Furthermore, a benchmark rat anti-mTNFR2 clone HM102 (Abcam, ab7369) with unknown blocking activity was included together with a rat IgG2a mAb (clone EBR2a) (eBioscience, 14-4321-85) as a negative control. Each time that binding and blocking experiment was performed, a gating for TNFR2 expression for FACS signal was performed with unstained CHO-K1.mTNFR2 cell line (Sup. Fig. 1 A), and in parallel TNFR2 expression was assessed (Sup. Fig. 1; B and C). mTNFR1 expression was assessed by anti-mTNFR1 PE antibody (Biolegend, 113003) and only detected following transfection with the mTNFR1 construct (Suppl. Fig. 1 D).

The stained cells were analysed on a FACS CantoTM II (BD) using the software program BD FACSDiva. Ten thousand events were counted. Further analysis was performed with FlowJo and shown results plotted in GraphPad.

2.6 Bio-Layer interferometry (BLI)

Antibody binding kinetics towards mouse TNFR2 were evaluated by bio-layer interferometry (BLI) using an Octet Red96 (Forte-Bio) in triplicates. First, the dissociation rate constant of 28 anti-mTNR2 antibodies derived from hybridoma supernatant was assessed (data not shown).

To assess mAbs kinetics, the affinity constant (K_D) toward recombinant mTNFR2 protein was determined. Rat anti-mTNFR2 purified antibodies were diluted (10 µg/mL) in 10mM acetate pH 5.0 and loaded on NHS/EDC activated Amine Reactive 2nd Generation (AR2G)(Forte-Bio,

18-5088). Thereafter, the antibody loaded biosensors were blocked with 1M ethanolamine (Forte-Bio, 18-1071). First, a single estimation screening of K_D value was performed with an expected saturating concentration of 100nM His tagged mTNFR2 (R&D Systems, 426-R2/CF) 100nM diluted in 10x Kinetics Buffer (KB) followed by a dissociation step. Based on the estimated K_D, the experiment was repeated three times per candidate starting with a recombinant mTNFR2 concentration 10 or 5 times above the single estimated K_D followed by 2-fold decreasing concentration dilution. Binding kinetics were measured by Octet system according to the manufacturer's instructions (ForteBio). Data was analysed using Data analysis software HT V10.0 (ForteBio).

2.7 Epitope mapping

Mouse-human TNFR2 chimeras were designed based on four different cysteine-rich domains (CRD) swap mutants: hTNFR2 (mCRD1), hTNFR2 (mCRD2), hTNFR2 (mCRD3), hTNFR2 (mCRD4), mTNFR2 (hCRD1), mTNFR2 (hCRD2), mTNFR2 (hCRD3) and mTNFR2 (hCRD4). mTNFR2, hTNFR2, and mTNFR1 were also included in the study. The N-terminal region for CRD1 and the C-terminal region following CRD4 was included as part of the respective domains. cDNA constructs were synthesized (GeneArt) and were subcloned with DH5α competent cells (Invitrogen, 18265-017) and amplified with GenElute HP plasmid Midiprep Kit (Sigma Aldrich, NA0200). Each construct was expressed after transient transfection of CHO-K1 cells using Lipofectamine 2000 (Invitrogen, 11668-019). After 6h hours with incubation media, cells were detached, and 5 x 10^6 cells were seeded per 96-wells f-bottom plates (Thermo Scientific, 150350) in final volume of 50 µL per well. Cells were incubated at 37 °C with 5% CO2 and 95% humidity for 16 hours. Afterwards, cells were incubated with 10-fold increasing concentrations (max 5 µg/mL) of anti-mTNFR2 mAbs diluted in CHO medium at 4 °C for 1 h and after 3 wash cycles with PBS 0,05% Tween-20 (VWR, 663684B), binding was detected with anti-rat IgG HRP 1:5000 (Jackson Immuno

Research, 112-035-167). After 3 wash cycles with PBS 0,05% Tween-20, TMB (Invitrogen) was added and after 15 min, reaction was stopped with 0.5M H_2SO_4. OD 450-620 was measured on Spectramax 340PC reader. Collected data was analysed in GraphPad Prism.

2.8 Treg staining

Binding of all anti-mTNFR2 mAbs was assessed on flow-sorted CD4+Foxp3/YFP+ cells from B6.129(Cg)-Foxp3tm4(YFP/cre)Ayr/J mice[33]. Spleens from FoxP3/YFP mice were homogenized and RBC lysed using the 1X RBC lysis buffer (Sigma Aldrich, R7757). Splenocytes were seeded at 2 x 10^6 cells/ml per 96-wells u-bottom plates (Thermo Scientific, 163320) in final volume of 50 µL per well. Two different staining procedures were followed: (i) Treg staining with generated anti-mTNFR2 antibodies and (ii) Treg staining with generated anti-mTNFR2 antibodies competing with benchmark anti-mTNFR2 (clone TR75-89, TNFα non-blocking).

i) Splenocytes were washed once with PBS 1% BSA (Sigma Aldrich, A7409) (FACS buffer). Cells were incubated at 4 °C for 30 min with 20 µg/mL of anti-mTNFR2 mAbs diluted in FACS buffer. Commercial hamster anti-mTNFR2 direct labelled with PE (clone TR75-79)(Biolegend, 113405) and hamster isotype control direct labelled with PE (BD Biosciences, 553972) were included as controls following manufacturer's concentrations. After 3 wash steps, cells were incubated at 4 °C for 30 min with hamster 5 µg/mL of anti-CD3-PE/Cy7 (Clone 145-2C11)(Biolegend, 100320) and mTNFR2 binding was detected with goat 4 µg/mL of anti-rat IgG-AF647 (Invitrogen, A21247).

ii) Similarly, splenocytes were washed once with PBS 1% BSA (Sigma Aldrich, A7409) (FACS buffer). Cells were incubated at 4 °C for 30 min with 20 µg/mL of anti-mTNFR2 mAbs diluted in FACS buffer. After 3 wash step, cells were incubated at 4 °C for 30 min with hamster 5 µg/mL of anti-CD3-PE/Cy7 (Clone 145-2C11)(Biolegend, 100320) and 2,5 µg/mL of

hamster anti-mouse CD120b (TNFR Type II/p75) -PE, (clone TR75-89) (Biolegend, 113405). Followed by 3 wash step, a third incubation at 4 °C for 30 min was performed to detect mTNFR2 binding with goat 4 μg/mL of anti-rat IgG AF647 (Invitrogen, A21247) assessing if both anti-mTNFR2 gave double positive signal.

Each replicate the gating strategy for TNFR2 expression obtained by FACS signal was performed with (i) rat isotype control (Sup. Fig. 2 A) and (ii) rat isotype control together with anti-mTNFR2-PE clone TR75-89. The stained cells were analysed on a FACS LSRFortessa (BD) using the software program BD FACSDiva. Further analysis was performed with FlowJo and shown results plotted in GraphPad.

2.9 CD8 staining

Binding of all anti-mTNFR2 mAbs was assessed on flow-sorted activated CD8+ cells from OT1 hom Rag1 KO mice, endogenously expressing mTNFR2 cells upon activation. Spleens from OT1 home Rag1 KO mice were homogenized and RBC lysed using the 1X RBC lysis buffer (Sigma Aldrich, R7757). Splenocytes were activated with 1:1000 SIINFKEL peptide and seeded at 0,5 x 10^6 cells/ml per 12 wells plates (Corning, 353043) in final volume of 1ml per well with IMDM complete medium (Sigma, I3390). Cells were for incubated for 2 days at 37 °C in 8% CO_2. Cells were split 1:2 at day two and used at day 3.

Activated OT1 cells were washed once with PBS 1% BSA (Sigma Aldrich, A7409) (FACS buffer). Cells were incubated at 4 °C for 30 min with 20 μg/mL of anti-mTNFR2 mAbs diluted in FACS buffer. Commercial hamster anti-mTNFR2 direct labelled with PE (clone TR75-79)(Biolegend, 113405) and hamster isotype control direct labelled with PE (BD Biosciences, 553972) were included as controls following manufacturer's concentrations. After 3 wash steps, cells were incubated at 4 °C for 30 min with human 1 μg/mL of anti-CD8-PerCP-Vio700

(Clone REA793)(Miltenyi Biotec, 130-111-637) and mTNFR2 binding was detected with goat 1 µg/mL of anti-rat IgG-PE (BD Biosciences, 550767).

The gating strategy for TNFR2 expression obtained by FACS signal was performed with a rat isotype control (gating strategy not shown). The stained cells were analysed on a FACS Canto (BD) using the software program BD FACSDiva. Further analysis was performed with FlowJo.

2.10 In vitro CD8+ T lymphocyte costimulation assay

Mouse CD8+ T lymphocytes were isolated from total splenocytes of C57BL/6J mice with CD8+ T cell isolation kit (MACS Miltenyi Biotec, 130-104-075) following manufacturer's instructions. Afterward, CD8+ T cells were costimulated at 37 °C with 5% CO2 and 95% for 72 h with preincubated plate-bound at 4 °C for 48 hours with Purified anti-mouse CD3 antibody (0.5 µg/mL, clone 17A2)(BioLegend, 100314) and anti-TNFR2 (2-fold decreasing concentrations starting at 50 µg/mL, generated Abs) at 1 x 10^6 cells/mL cultured in RPMI (Gibco, 61870-010) supplemented with 100 U/mL Penicillin, 100 µg/mL Streptomycin (Gibco, 15140-122), 50 µM 2-mercaptoethanol (Gibco, 31350-010), and 10% FBS (Life Technologies, 10270106). Costimulation with 0.5 µg/mL anti-CD3 antibody and 5 µg/mL purified anti-mouse CD28 antibody (clone E18)(Biolegend, 122004) was taken as a positive control. Single stimulation with 0.5 µg/mL anti-CD3e was taken as a reference control and isolated CD8+ T cells without any stimulation were considered as negative control. After 72 hours, IFN-γ present in media was measured via Mouse IFN-γ ELISA Set (BD Biosciences, 555138) to assess co-stimulatory capacity following manufacturer's instructions. Collected data of the experiment performed twice was analysed, where wells containing just media were considered as a blank. IFNγ was calculated based on the standard curve after blank subtraction, and values derived per plate from anti-CD3 incubation were normalized as 0% value of costimulation and values derived from anti-CD3 + anti-CD28 incubation were considered as a 100% signal of costimulation.

3. Results

3.1 Generation of a panel of anti-mouse TNFR2 mAbs

Novel antibodies that bind specifically to murine TNFR2 were generated in rats by mTNFR2 gene gun immunization. Following anti-TNFR2 B-cell enrichment, B-cell expansion, and subsequent B-cell lead selection formini-electrofusion led to a set of 13 hybridomas producing distinct anti-mTNFR2 mAbs. Isotyping results revealed that all the produced antibodies were rat IgG2a isotype (data not shown). In order to assess protein quality of each anti-TNFR2 antibody, antibodies were purified and characterized using several analytical procedures. SEC-UPLC analysis showed good monomericity between 95.3% and 99.5% for each of the 13 selected candidates (Sup. Table 2). While freeze and thaw cycles had no significant impact on protein monomericity with values higher than 98%, incubation at 40 °C for one week affected the quality of some candidates leading to aggregates formation with monomericities from 45.2% of candidate 16A to 93.8% of candidate 18A (Sup. Table 2). Furthermore, CE-SDS analysis confirmed proper assembly of heavy and light chain the percentage of intact IgG being more than 90% in all samples (Sup. Table 2, Sup. Fig. 3).

3.1 α-mTNFR2 mAbs present different cell binding and blocking activity

Mean binding activity was assessed on mTNFR2 stably transfected CHO-K1 cell line (Fig. 1 A, B). Benchmark rat anti-mTNFR2 was included as a positive control together with a rat IgG2a mAb isotype as a negative control. Based on the binding plateau (efficacy), mAbs candidates could be divided in two groups. While most of the candidates reach plateau around 7500 gMFI, candidates 5A, 10A, 14A, 18A and 26A present lower efficacy achieving approximately 2500 gMFI. Among those showing equal efficacy, monoclonal antibody candidates presented with different potency (mAb concentration at which 50% of maximum signal is observed (EC50)) ranging from 0.07 nM up to 3.75 nM. Candidate 14 with an EC50 of 16.41 nM is not represented by full S-shaped curve; mAb 8A is the most efficacious and

potent, presenting the lowest EC50, 0.07 nM (Table 1). The affinity of purified anti-mTNFR2 antibodies for binding to recombinant monomeric mTNFR2 was quantified using bio-layer interferometry (BLI). Assessment of binding kinetics showed fast on-rate for most antibodies, resulting in K_D values ranging from 2.7 to 56.8 nM (Table 1). A fully characterization for binding kinetics from candidate 14A was not achieved, most likely because of technical limitations explained at least in part by its low binding efficiency.

Next, the blocking activity of the mAb candidates was evaluated by flow cytometry using recombinant biotinylated TNFα for binding to CHOK1.mTNFR2 cells. Purified clone TR75-54.7 listed as blocking and clone TR75-89 listed as a non-blocking anti-TNFR2 mAb were taken as a reference. Candidates 8A, 12A, 16A, 25A, and 29A were able to block TNFα binding either partially or completely (Fig. 1 C), with candidate 25A showing the most potent (0.40 nM) blocking activity, assessed by the IC50, (Fig. 1 C) compared to 2.59 nM for the blocking benchmark antibody (data not shown). Based on these results, candidates 8A, 16A, and 29A are considered partial blockers as all presented more than 50% reduction of signal (Fig. 1 C). Candidates that showed less than 25% of reduction of signal compared to the benchmark hamster anti-mTNFR2 non-blocking antibody are considered non-blocking antibodies (Sup. Fig. 1 E).

In summary, a panel of thirteen novel anti-mTNFR2 antibodies with different biophysical properties, varying binding affinity to mTNFR2 and varying TNFα ligand blocking potency were identified.

3.2 Mapping of mTNFR2 binding domains

Cysteine-Rich Domains (CRDs) of human TNFR2 were replaced by their cognate mouse regions and vice versa and subsequently expressed on CHO cells (Fig. 2 A, Sup. Fig. 4 A).

This reciprocal set-up allows to study the mCRD binding domains for each anti-TNFR2 antibody. CHO empty vector and mTNFR1 were also included (Sup. Fig 4 B).

Binding to mTNFR2 constructs with individual human CRD domains swapped in, respectively, was taken as a reference for each candidate (Fig. 2 B).

Candidate 14A was determined to be cross-reactive to human mTNFR2 (Fig. 2 B), it bound to all the constructs. Based on domain swapping, candidates 5A, 6A and 8A bound to mCRD1. The epitope of these mCRD1-binding candidates might include the N-terminal region, as this was included in the CRD1 swap mutants. Candidates 12A, 16A, 18A, 29A bound to mCRD2, similar to the benchmark rat anti-mTNFR2 clone HM102. Candidates 10A, 15A, 25A, 26A, and 30A were found to bind to mCRD3. None of the candidates bind to mCRD4 (most proximal to the cell membrane). The binding activity data for the reverse set-up (individual hCRD domains grafted in mTFR2) is shown in Sup. Fig. 4 B. By this analysis, the benchmark rat anti-mTNFR2 clone HM102 was shown to bind to a region containing parts of mCRD1 and mCRD2 (Fig. 2 B), and confirming the same binding region for all generated antibodies as observed in the previous set-up. None of the candidates presented cross-reactivity to mTNFR1 (Sup. Fig. 4 B). Rat IgG2a isotype control was taken as a negative control and presented no binding to any of the studied conditions (Sup. Fig. 4 C). The binding site of the novel rat anti-mouse TNFR2 antibodies was mapped to the extracellular CRDs as graphically displayed onto the human TNFR2:TNFα complex PDB structure (PDB ID: 3ALQ) summarized in Figure 2 C, with a sequence homology of 74% thought to be highly structurally similar.

Similarly to other TNFR superfamily members[34], CRD2 and CRD3 of mouse TNFR2 are the most important for ligand binding[35,36]. Blocking antibodies 12A, 16A and 29A were able to block TNFα binding, which is consistent with their binding region overlapping with the ligand interface in CRD2. Along a similar line of reasoning, the most potent and efficacious blocking

antibody was candidate 25A mapped to bind to CRD3. Candidate 18A, which presented binding to mCRD2, and candidates 10A, 15A, 26A, and 30A which presented binding to mCRD3, do not display blocking activity. Interestingly, candidate 8A presented TNFα blocking activity despite its binding to CRD1 which is outside of the ligand interface. Altogether, a diverse set of thirteen antibodies was identified targeting three mTNFR2 CRDs.

3.3 α-mTNFR2 mAbs stain mouse splenic Tregs and CD8+ cells

To verify whether this panel of anti-mTNFR2 antibodies is attractive to explore the role and activity of TNFR2 on immune cells *in vivo*, flow cytometry mAb staining on mouse Treg cells was assessed *ex vivo* using spleen-derived Tregs identified by YFP expression (FoxP3-YFP transgenic mice[33]). All candidates were found to stain YFP+ mouse Tregs (Fig. 3 A) and activated CD8+ cells (Fig. 3B). While the most potent binders detected Tregs and activated CD8+ cells with a clear shift on the flow cytometer (up to ~95% TNFR2+), some candidates (5A, 10A, 18A and 26A) displayed a weaker signal (~10% TNFR2+) (gMFI for mTNFR2 Treg binding shown in Sup. Table 3).

Furthermore, competitive binding to TNFR2 was assessed using the hamster-anti-mTNFR2 clone TR75-89 known to stain mouse Tregs[37]. In a competitive flow cytometry assay using YFP+ mouse Tregs, two different staining profiles were observed as expected, exemplified by 8A that directly competed and suppressed the TR75-89 signal, whereas 25A displayed concurrent binding to mouse TNFR2 indicating a different epitope (Fig. 3 C). Antibodies 5A and 18A appeared to outcompete the benchmark antibody for binding to Tregs but did not generate a strong signal themselves, (Sup. Table 3). Overall, all anti-rat TNFR2 antibodies characterized in this panel detected and stained splenic Treg cells *ex vivo*.

3.4 A selection of α-mTNFR2 antibodies shows capacity to costimulate CD8+ T-cells

In addition to CD28, several TNFRSF family members are able to generate an alternative co-stimulatory signal *in vivo*[38]. Therefore, we explored the potential of our panel of antibodies for their capacity to costimulate $CD8^+$ T-cells *ex vivo*. Using suboptimal anti-CD3 plus each anti-mTNFR2 antibody coated onto assay plates, the co-stimulatory activity of our antibody panel was assessed by reading out IFNγ production from freshly isolated splenic $CD8^+$ T-cells.

Results were normalized against optimal costimulation achieved using anti-CD28 (set at 100%). Some of our anti-mTNFR2 antibodies displayed co-stimulatory capacity on $CD8^+$ T-cells at a coating concentration of 50 µg/mL (Fig. 3 D). Notably, 15A demonstrated reproducible co-stimulatory capacity in independent experiments and across individual mice. Similarly, 5A, 10A, 18A, 26A and 30A appear to display varying co-stimulatory activity, albeit only in some of the experiments. Antibodies 6A, 8A, 12A, 14A and 29A did not show co-stimulatory activity in three consecutive independent experiments.

Therefore, although most of the antibodies did not demonstrate robust activity towards mouse $CD8^+$ T-cells, few candidates presented reproducible $CD8^+$ T cell, highlighting candidate 15. Surprisingly, these were characterized to bind different CRDs on mouse TNFR2.

4. Discussion

TNFR2 function affects multiple signaling pathways and cell states. However, it is still not entirely clear what critical activity TNFR2 has on different immune cells, and this may explain the substantial controversy that exists regarding the question as to how to target this receptor in disease[39,40].

The lack of well-characterized and available antibody reagents against mouse TNFR2 prompted us to generate a novel panel of thirteen rat anti-mouse TNFR2 antibodies to support more definitive exploration of TNFR2 in mouse models of disease.

These thirteen candidates can be classified based on their properties, all of them presenting distinct features. While all of them bind to mTNFR2, only candidate 14A has been shown to be cross-reactive to human TNFR2. However, this hallmark of 14A may be convoluted by a reduced potency and efficacy of mTNFR2 binding, rendering it difficult to explore further. Candidates 8A and 25A presented the highest efficacy of binding to CHO-K1.mTNFR2 based on absolute MFI, whereas mAbs 5A, 10A, 14A, 18A, and 26A were ranked with the lowest one. K_D values ranging from 2.7 to 56.8 nM presented 1-2 orders of magnitude lower EC50 of binding compared to EC50 determined of binding to native protein expressed on CHO-K1 cells, presumably because BLI experiments were set up to detect monovalent binding (affinity) while binding experiments by flow cytometry included bivalent binding (avidity). With the exception of candidates 16A and 18A, antibodies with reduced K_D to recombinant protein also demonstrated reduced binding efficacy to TNFR2 expressed on cells, suggesting the latter could be a result of relative fast dissociation of the mAb.

Five candidates present TNFα blocking activity. For candidates 12A, 16A, 25A and 29A this result is consistent with epitope mapping to CRD2 or CRD3 (25A), whereas candidate 8A can compete with the ligand binding although it binds to different TNFR2 domain, CRD1, which is not known to interact with TNFα. Surprisingly, candidate 18A which presented binding to CRD2 does not present blocking activity. Blocking antibodies were found in all epitope bins, presumably because of steric hindrance or by conformational changes induced in the ligand binding domains in addition to direct blockade of ligand binding. An extensive study via protein modeling would help to understand these differences and the interaction of each antibody with the receptor.

The TNFR2 staining intensity on the Treg population marked by FoxP3 driven YFP expression and on activated CD8+ cells is proportional with antibody affinity. Their capacity to cause a clear shift in the flow cytometer largely correlated to binding on CHO-K1.mTNFR2: for

instance 5A and 18A did not generate a high gMFI on CHO-K1.mTNFR2 and demonstrate weak binding to mouse Tregs at the concentrations used in flow cytometry. Similarly, weak mTNFR2 binding on activated CD8+ cells is observed with candidates 5A and 18A. Most of the anti-mTNFR2 candidates demonstrated staining of mouse Treg TNFR2 when coincubated with hamster-anti-mTNFR2 clone TR75-89 antibody, with the exception of 6A, 8A (epitopes mapped to CRD1) and 10A (CRD2/3) that might compete for the same epitope or affect binding otherwise (steric hindrance, conformational change).

Several of the generated antibodies reproducibly demonstrated costimulation of mouse $CD8^+$ T-cells *in vitro*. Costimulatory anti-mTNFR2 antibodies were found to bind across multiple epitope bins (5A, 15A, 18A mapped to CRD1, CRD3, CRD2, respectively). Further study of protein structure by crystallography could potentially help explain which antibody features might explain blocking or costimulatory activity towards mTNFR2. Despite the lack of this information, studying the biology triggered upon anti-TNFR2 binding on TNFR2 on cell surface is an interesting approach to be explored in cancer and autoimmune disease field. Using the antibody characteristics described in this study, it would make sense to explore whether they display the ability to modulate TNFR2-dependent pharmacology *in vitro* and *in vivo*. For example, in experimental autoimmune encephalomyelitis (EAE), TNFR2 stimulation was shown to promote oligodendrocyte differentiation and remyelination[41] and increase numbers of Tregs which would reduce the number of pathogenic T conventional cells[42]. Therefore, it could be interesting to confirm activity of 15A in this model, and compare it to non-(co-) stimulatory candidates. Similarly, highlighting its crucial role in maintaining an immunosuppressive tumor microenvironment, blocking the TNFα-TNFR2 axis on Tregs and myeloid-derived suppressor cells, or depleting TNFR2 expressing cells appears to be a promising treatment in cancer. Consequently, for this purpose, it would be more convenient to select one of the TNFα blocking antibodies. Furthermore, as a potential strategy to enhance

tumor immunity Fc-mediated depletion of TNFR2 expressing Tregs cells could be explored. However, since activated effector CD8 T cells also express TNFR2[43], this might require careful characterization of TNFR2 expression in tumor microenvironment to find a potential therapeutic window in time, enabling selective depletion of Tregs.

In conclusion, this novel anti-mouse TNFR2 antibody panel represents a useful tool to study TNFR2 biology *in vitro* and *in vivo* with potential applications in cancer and autoimmune diseases.

Study approval

The welfare of the mice was maintained in accordance with the general principles governing the use of animals in experiments of the European Communities (Directive 2010/63/EU) and Dutch legislation (The revised Experiments on Animals Act, 2014).

Funding details

This work was supported by the European Union's Horizon 2020 research and innovation programme under the Marie Skłodowska-Curie grant agreement [grant numbers 765394, 2018]. We thank T. Guyomard (Aduro Biotech Europe), J. Russo and D. Cuculescu (Cima Universidad de Navarra) for their expert technical assistance.

Disclosure statement

The authors declare no competing interests.

References

1. Kalfaoglu B, Almeida-Santos J, Tye CA, Satou Y, Ono M. T-Cell Hyperactivation and Paralysis in Severe COVID-19 Infection Revealed by Single-Cell Analysis. Front Immunol. 2020 Oct 8. doi: 10.3389/fimmu.2020.589380. PMID: 33178221

2. Callahan MK, Postow MA, Wolchok JD. Targeting T Cell Co-receptors for Cancer Therapy. Immunity. 2016 May 17. doi: 10.1016/j.immuni.2016.04.023. PMID: 27192570

524 3. Sade-Feldman M, Yizhak K, Bjorgaard SL, Ray JP, de Boer CG, Jenkins RW, et al.
525 Defining T Cell States Associated with Response to Checkpoint Immunotherapy in
526 Melanoma. Cell. 2019 Jan 10. doi: 10.1016/j.cell.2018.12.034 PMID: 30633907

527 4. Ramos-Casals M, Brahmer JR, Callahan MK, Flores-Chávez A, Keegan N, Khamashta
528 MA, et al. Immune-related adverse events of checkpoint inhibitors. Nat Rev Dis Primer.
529 2020 May 7. doi: 10.1038/s41572-020-0160-6. PMID: 32382051

530 5. Paluch C, Santos AM, Anzilotti C, Cornall RJ, Davis SJ. Immune Checkpoints as
531 Therapeutic Targets in Autoimmunity. Front Immunol. 2018 Oct 8. doi:
532 10.3389/fimmu.2018.02306. PMID: 30349540

533 6. Zhang Q, Vignali DAA. Co-stimulatory and co-inhibitory pathways in autoimmunity.
534 Immunity. 2016 May 17. doi: 10.1016/j.immuni.2016.04.017. PMID: 27192568

535 7. Mayes PA, Hance KW, Hoos A. The promise and challenges of immune agonist antibody
536 development in cancer. Nat Rev Drug Discov. 2018 Jul. doi: 10.1038/nrd.2018.75.
537 PMID: 29904196

538 8. Eskiocak U, Guzman W, Wolf B, Cummings C, Milling L, Wu H-J, et al. Differentiated
539 agonistic antibody targeting CD137 eradicates large tumors without hepatotoxicity. JCI
540 Insight. 2020 Mar 12. doi: 10.1172/jci.insight.133647. PMID: 32161196

541 9. Liu Z, Davidson A. BAFF inhibition: a new class of drugs for the treatment of
542 autoimmunity. Exp Cell Res. 2011 May 15. doi: 10.1016/j.yexcr.2011.02.005.
543 PMID: 21333645

544 10. Sonar S, Lal G. Role of Tumor Necrosis Factor Superfamily in Neuroinflammation and
545 Autoimmunity. Front Immunol. 2015 Jul 20. doi: 10.3389/fimmu.2015.00364.
546 PMID: 26257732

547 11. Ward-Kavanagh LK, Lin WW, Šedý JR, Ware CF. The TNF Receptor Superfamily in
548 Co-stimulating and Co-inhibitory Responses. Immunity. 2016 May 17. doi:
549 10.1016/j.immuni.2016.04.019. PMID: 27192566

550 12. Poggi M, Jager J, Paulmyer-Lacroix O, Peiretti F, Gremeaux T, Verdier M, et al. The
551 inflammatory receptor CD40 is expressed on human adipocytes: contribution to
552 crosstalk between lymphocytes and adipocytes. Diabetologia. 2009 Jun. doi:
553 10.1007/s00125-009-1267-1. PMID: 19183933

554 13. Lincecum JM, Vieira FG, Wang MZ, Thompson K, De Zutter GS, Kidd J, et al. From
555 transcriptome analysis to therapeutic anti-CD40L treatment in the SOD1 model of
556 amyotrophic lateral sclerosis. Nat Genet. 2010 May. doi: 10.1038/ng.557.
557 PMID: 20348957

558 14. van Mierlo GJD, den Boer AT, Medema JP, van der Voort EIH, Fransen MF, Offringa R,
559 et al. CD40 stimulation leads to effective therapy of CD40- tumors through induction of
560 strong systemic cytotoxic T lymphocyte immunity. Proc Natl Acad Sci. 2002 Apr 16.
561 doi: 10.1073/pnas.082107699. PMID: 11929985

562 15. Sandin LC, Orlova A, Gustafsson E, Ellmark P, Tolmachev V, Totterman TH, et al.
563 Locally Delivered CD40 Agonist Antibody Accumulates in Secondary Lymphoid

564 Organs and Eradicates Experimental Disseminated Bladder Cancer. Cancer Immunol
565 Res. 2014 Jan 1. doi: 10.1158/2326-6066. PMID: 24778163

566 16. Schling P, Rudolph C, Heimerl S, Fruth S, Schmitz G. Expression of tumor necrosis
567 factor alpha and its receptors during cellular differentiation. Cytokine. 2006 Mar 7. doi:
568 10.1016/j.cyto.2006.02.007. PMID: 16580225

569 17. Arnett HA, Mason J, Marino M, Suzuki K, Matsushima GK, Ting JP-Y. TNFα promotes
570 proliferation of oligodendrocyte progenitors and remyelination. Nat Neurosci. 2001
571 Nov. doi: 10.1038/nn738. PMID: 11600888

572 18. Irwin MW, Mak S, Mann DL, Qu R, Penninger JM, Yan A, et al. Tissue Expression and
573 Immunolocalization of Tumor Necrosis Factor-α in Postinfarction Dysfunctional
574 Myocardium. Circulation. 1999 Mar 23. doi: 10.1161/01.cir.99.11.1492.
575 PMID: 10086975.

576 19. Naserian S, Abdelgawad ME, Afshar Bakshloo M, Ha G, Arouche N, Cohen JL, et al.
577 The TNF/TNFR2 signaling pathway is a key regulatory factor in endothelial progenitor
578 cell immunosuppressive effect. Cell Commun Signal CCS. 2020 Jun 16. DOI:
579 10.1186/s12964-020-00564-3. PMID: 32546175.

580 20. Beldi G, Khosravi M, Abdelgawad ME, Salomon BL, Uzan G, Haouas H, et al.
581 TNFα/TNFR2 signaling pathway: an active immune checkpoint for mesenchymal stem
582 cell immunoregulatory function. Stem Cell Res Ther. 2020 Jul 16. DOI:
583 10.1186/s13287-020-01740-5 PMID: 32669116

584 21. Ware CF, Crowe P, Vanarsdale TL, Andrews JL, Grayson MH, Smith CA, et al. Tumor
585 necrosis factor (TNF) receptor expression in T lymphocytes. Differential regulation of
586 the type I TNF receptor during activation of resting and effector T cells. J Immunol.
587 1991 Dec 15.PMID: 1661312

588 22. Brenner D, Blaser H, Mak TW. Regulation of tumour necrosis factor signalling: live or
589 let die. Nat Rev Immunol. 2015 Jun. DOI: 10.1038/nri3834 . PMID: 26008591

590 23. He J, Li R, Chen Y, Hu Y, Chen X. TNFR2-expressing CD4+Foxp3+ regulatory T cells
591 in cancer immunology and immunotherapy. Prog Mol Biol Transl Sci. 2019 Apr 10. doi:
592 10.1016/bs.pmbts.2019.03.010. PMID: 31383403

593 24. Chen X, Subleski JJ, Hamano R, Howard OMZ, Wiltrout RH, Oppenheim JJ. Co-
594 expression of TNFR2 and CD25 identifies more of the functional CD4 + FOXP3 +
595 regulatory T cells in human peripheral blood: Immunomodulation. Eur J Immunol. 2010
596 Apr 14. doi: 10.1002/eji.200940022. PMID: 20127680

597 25. Zhao T, Li H, Liu Z. Tumor necrosis factor receptor 2 promotes growth of colorectal
598 cancer via the PI3K/AKT signaling pathway. Oncol Lett. 2017 Jan. doi:
599 10.3892/ol.2016.5403. PMID: 28123565

600 26. Kim EY, Teh S-J, Yang J, Chow MT, Teh H-S. TNFR2-Deficient Memory CD8 T Cells
601 Provide Superior Protection against Tumor Cell Growth. J Immunol. 2009 Nov 15. doi:
602 10.4049/jimmunol.0803482. PMID: 19841176

27. Hurrell BP, Galle-Treger L, Jahani PS, Howard E, Helou DG, Banie H, et al. TNFR2 Signaling Enhances ILC2 Survival, Function, and Induction of Airway Hyperreactivity. Cell Rep. 2019 Dec 24. doi: 10.1016/j.celrep.2019.11.102. PMID: 31875557

28. Atretkhany K-SN, Mufazalov IA, Dunst J, Kuchmiy A, Gogoleva VS, Andruszewski D, et al. Intrinsic TNFR2 signaling in T regulatory cells provides protection in CNS autoimmunity. Proc Natl Acad Sci. 2018 Dec 18. doi: 10.1073/pnas.1807499115. PMID: 30498033

29. Naserian S, Shamdani S, Arouche N, Uzan G. Regulatory T cell induction by mesenchymal stem cells depends on the expression of TNFR2 by T cells. Stem Cell Res Ther. 2020 Dec 10. DOI: 10.1186/s13287-020-02057-z. PMID: 33303019

30. Voets E, Paradé M, Lutje Hulsik D, Spijkers S, Janssen W, Rens J, et al. Functional characterization of the selective pan-allele anti-SIRPα antibody ADU-1805 that blocks the SIRPα–CD47 innate immune checkpoint. J Immunother Cancer. 2019 Dec 4. doi: 10.1186/s40425-019-0772-0. PMID: 31801627

31. Steenbakkers PGA, Hubers HAJM, Rijnders AWM. Efficient generation of monoclonal antibodies from preselected antigenspecific B cells. Mol Biol Rep. 1994 Mar 1. doi: 10.1007/BF00997158. PMID: 8072493

32. Steenbakkers PGA, van Meel FCM, Olijve W. A new approach to the generation of human or murine antibody producing hybridomas. J Immunol Methods. 1992 Jul 31. doi: 10.1016/0022-1759(92)90090-G

33. Williams LM, Rudensky AY. Maintenance of the Foxp3-dependent developmental program in mature regulatory T cells requires continued expression of Foxp3. Nat Immunol. 2007 Jan 14. doi: 10.1038/ni1437. PMID:17220892

34. Locksley RM, Killeen N, Lenardo MJ. The TNF and TNF receptor superfamilies: integrating mammalian biology. Cell. 2001 Feb 23. doi: 10.1016/s0092-8674(01)00237-9. PMID: 11239407.

35. Banner DW, D'Arcy A, Janes W, Gentz R, Schoenfeld HJ, Broger C, et al. Crystal structure of the soluble human 55 kd TNF receptor-human TNF beta complex: implications for TNF receptor activation. Cell. 1993 May 7. doi: 10.1016/0092-8674(93)90132-a. PMID: 8387891

36. Mukai Y, Nakamura T, Yoshikawa M, Yoshioka Y, Tsunoda S, Nakagawa S, Yamagata Y, Tsutsumi Y. Solution of the structure of the TNF-TNFR2 complex. Sci Signal. 2010 Nov 16. doi: 10.1126/scisignal.2000954. PMID: 21081755.

37. Williams GS, Mistry B, Guillard S, Ulrichsen JC, Sandercock AM, Wang J, et al. Phenotypic screening reveals TNFR2 as a promising target for cancer immunotherapy. Oncotarget. 2016 Oct 18. doi: 10.18632/oncotarget.11943. PMID: 27626702.

38. Teijeira A, Labiano S, Garasa S, Etxeberria I, Santamaría E, Rouzaut A, et al. Mitochondrial Morphological and Functional Reprogramming Following CD137 (4-1BB) Costimulation. Cancer Immunol Res. 2018 Jul. doi: 10.1158/2326-6066.CIR-17-0767. PMID: 29678874.

643 39. Medler J, Wajant H. Tumor necrosis factor receptor-2 (TNFR2): an overview of an
644 emerging drug target. Expert Opin Ther Targets. 2019 Apr 3. doi:
645 10.1080/14728222.2019.1586886. PMID: 30856027

646 40. Fischer R, Kontermann RE, Pfizenmaier K. Selective Targeting of TNF Receptors as a
647 Novel Therapeutic Approach. Front Cell Dev Biol. 2020 May 26. doi:
648 10.3389/fcell.2020.00401. PMID: 32528961

649 41. Madsen PM, Motti D, Karmally S, Szymkowski DE, Lambertsen KL, Bethea JR, et al.
650 Oligodendroglial TNFR2 Mediates Membrane TNF-Dependent Repair in Experimental
651 Autoimmune Encephalomyelitis by Promoting Oligodendrocyte Differentiation and
652 Remyelination. J Neurosci. 2016 May 4. doi: 10.1523/JNEUROSCI.0211-16.2016.
653 PMID: 27147664

654 42. Ronin E, Pouchy C, Khosravi M, Hilaire M, Grégoire S, Casrouge A, et al. Tissue-
655 restricted control of established central nervous system autoimmunity by TNF receptor
656 2–expressing Treg cells. Proc Natl Acad Sci. 2021 Mar 30. doi:
657 10.1073/pnas.2014043118. PMID: 33766913

658 43. Calzascia T, Pellegrini M, Hall H, Sabbagh L, Ono N, Elford AR, et al. TNF-α is critical
659 for antitumor but not antiviral T cell immunity in mice. J Clin Invest. 2007 Nov 8. doi:
660 10.1172/JCI32567. PMID: 17992258

661

662

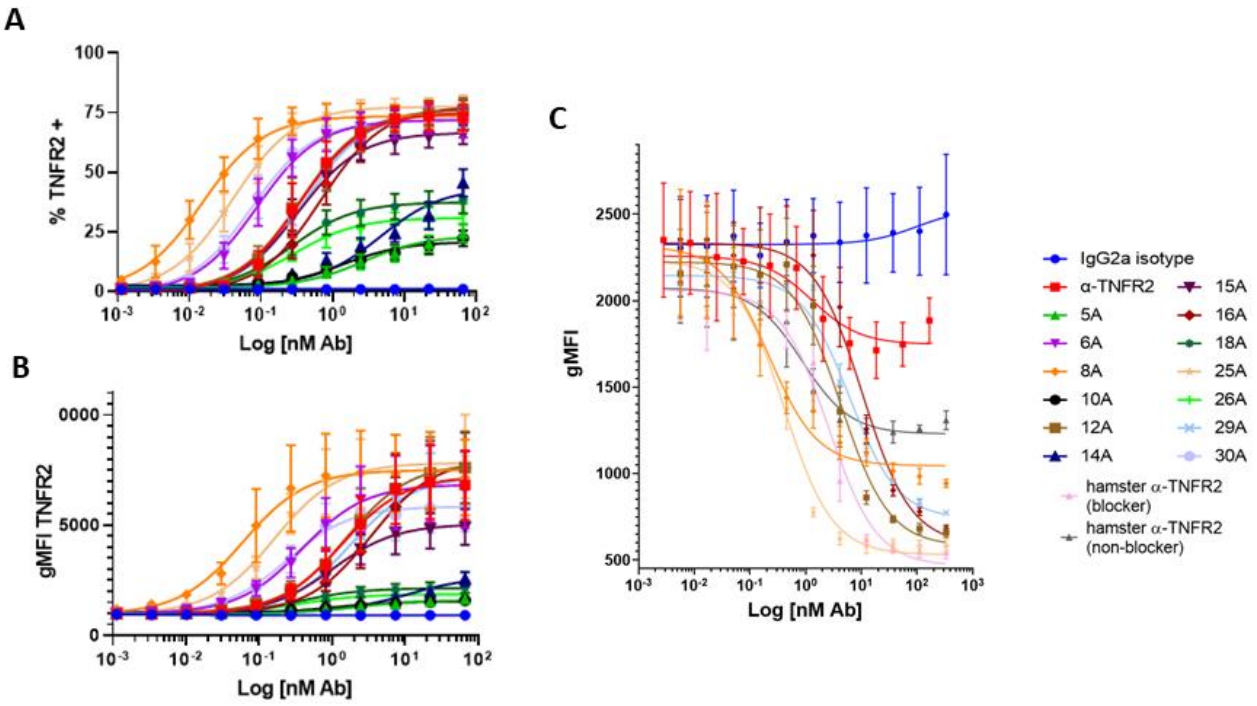

Figure 1. Characterization of anti-mouse TNFR2 antibodies in vitro. (A and B) mTNFR2 stable transfected CHO-K1 cells were incubated with 3-fold increasing concentrations of each rat IgG2a mAbs, and binding was detected by flow cytometry assessing TNFR2 + population percentage (A) and gMFI (B). (C) TNFα ligand competition with generated antibodies assessed by FACS. Data represented as a three-parameter gMFI dose-response curve fit of the blocker antibodies with appropriate controls incubations with 3-fold increasing concentrations. Two benchmark hamster-anti-mTNFR2 antibodies with known blocking activity were added as controls. All data based on mean and SEM is representative of three independent experiments.

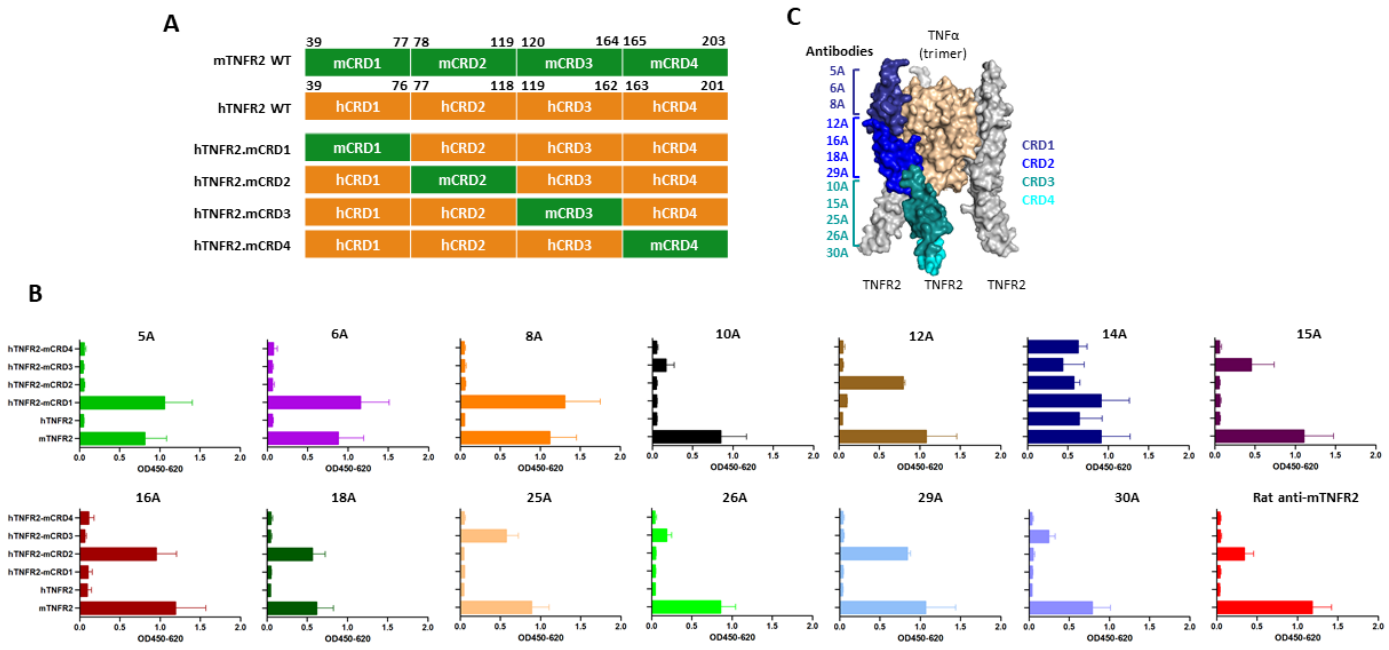

674

675 **Figure 2.** Characterization of anti-mTNFR2 mAbs targeting CRDs 1-4. (A) Schematic
676 representation of the 6 mouse-human TNF2 chimeras CRD1-CRD4 (Cystein Rich Domain).
677 (B) The targeting CRD of each mAb were determined by cell ELISA with mouse-human
678 TNFR2 domain swap mutants. Data represented as a three-parameter OD450-620 detection
679 based on mean and SD of three independent experiments. (C) The domain epitopes of the 13
680 mAbs are indicated on a hTNFR2-hTNFα trimer structure (PDB: 3ALQ), 74% similar to mouse
681 TNFR2. The CRDs for one TNFR2 receptor are shown in indicated colors.

682

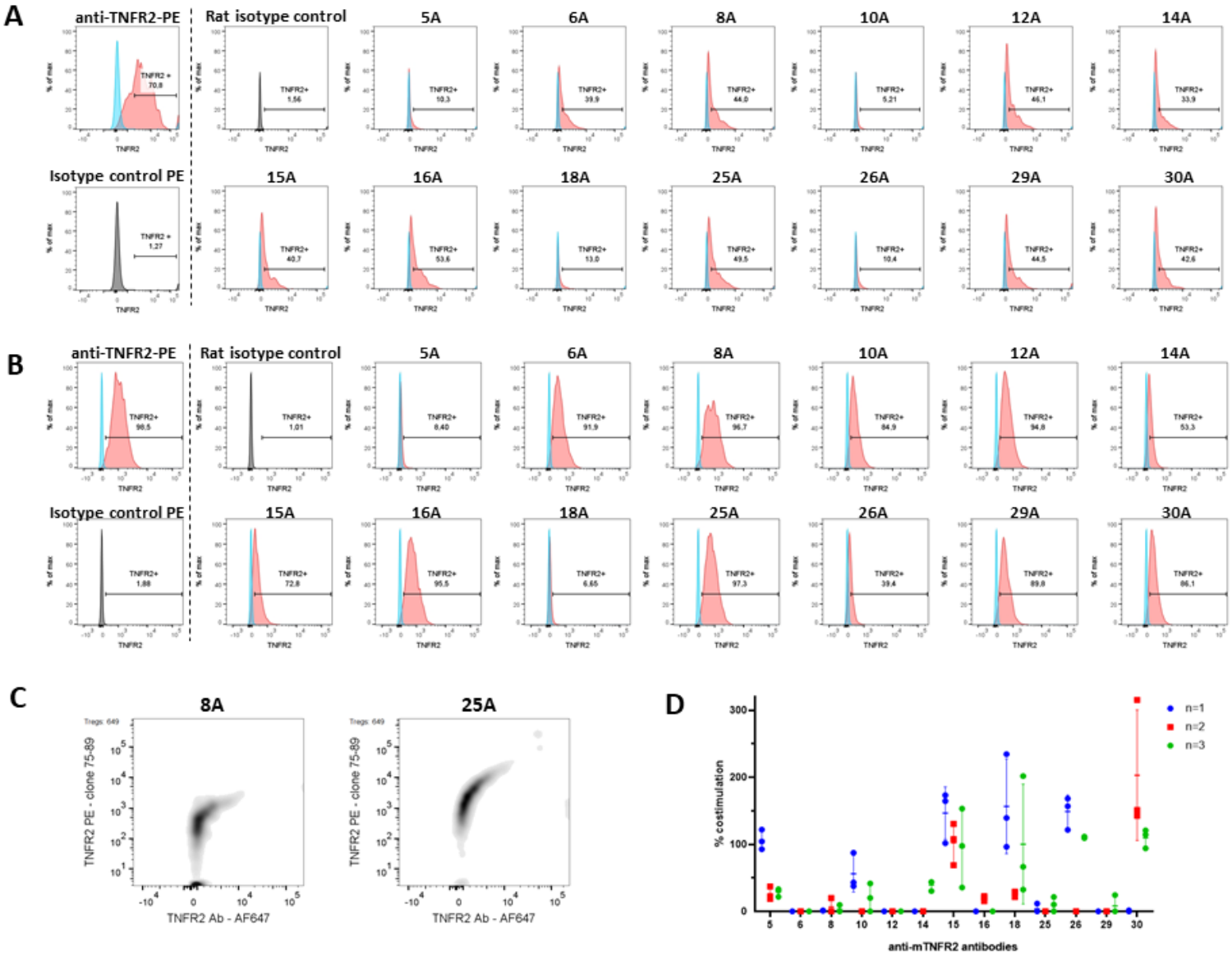

683

684 **Figure 3.** Characterization of anti-mouse TNFR2 antibodies with ex vivo material. (A) TNFR2
685 expression upon binding of anti-mTNFR2 antibodies to Treg cell population. Detection by
686 commercial hamster anti-TNFR2 direct labeled with PE with the respective hamster-isotype
687 control labeled with PE (left). Generated rat anti-mTNFR2 antibodies and a rat isotype control
688 were detected by a secondary antibody anti-rat AF647 label (right). Gating strategy shown in
689 (Sup. Fig. 2 A) The isotype control has been overlaid in each anti-mTNFR2 antibody histogram
690 represented with % of max. Data representative of two independent experiments. (B) TNFR2
691 expression upon binding of anti-mTNFR2 antibodies to activated CD8+ cells. Detection by

commercial hamster anti-TNFR2 direct labeled with PE with the respective hamster-isotype control labeled with PE (left). Generated rat anti-mTNFR2 antibodies and a rat isotype control were detected by a secondary antibody anti-rat PE label (right). Gating strategy not shown. Gating strategy for CD8+ population was done on unstained OT1 activated cells. First, OT1 cells were gated based on FSC-A / SSC-A properties. Next, single cells were gated based FSC-A / FSC-H. CD8+ population were gated as CD8-PerCP-Vio700 positive. Next to the CD8+ population, a mouse TNFR2+ gate was set with a rat isotype control via histogram. The isotype control has been overlaid in each anti-mTNFR2 antibody histogram represented with % of max. Data representative of single experiment out of two independent experiments. (C)TNFR2 expressing Treg cells co-staining, representation of candidates 18 and 25 with a benchmark antibody, clone TR75-89. Data representative of two independent experiments. (D) Costimulation of CD8+ T-cells with anti-TNFR2 antibodies. Assessment of *in vitro* CD8+ T-cell costimulation for different anti-TNFR2 antibodies (plate bound anti-CD3 at 0.5 µg/mL). Anti-TNFR2 antibodies were plate bound in 2-fold decreasing dilution starting at 50 µg/mL. Data representative of three independent experiments with n=3 biological replicates on the read out of IFNγ in supernatant at 50 µg/mL per each candidate and mean of independent experiment. Blank was subtracted, IFNγ was calculated based on the standard curve and normalized based on single incubation of anti-CD3 antibodies as 0% costimulation and double incubation of anti-CD3 + anti-CD28 antibodies as a 100% costimulation.

Table 1. EC50, IC50 and binding kinetics. Summary of EC50 based on gMFI of binding and report of TNFa blocker or non-blocker antibodies showing which IC50 values for the blocker ones, based on gMFI. Binding kinetics based on Kon, Koff and KD. Values shown in nM result from the mean of three independent experiments ± standard deviation. N.A., non- available. (*) Value obtained without full S-shaped curve reaching the maximum baseline.

anti-mTNFR2 mAbs	EC50 binding (nM ± SD)	mTNFα blocker	IC50 blocking (nM ± SD)	Kon average (1/Ms) ± SD)	Koff average (1/s) ± SD)	KD average (nM ± SD)
5A	1,90 ± 0,001 *	No	-	3,96E+05 ± 9,22E+04	1,87E-02 ± 1,74E-03	49,3 ± 13,5
6A	0,39 ± 0,061	No	-	2,34E+05 ± 6,35E+04	1,14E-03 ± 5,42E-04	4,8 ± 1,7
8A	0,07 ± 0,033	Yes	0,22 ± 0,07 *	3,49E+05 ± 8,22E+04	4,14E-03 ± 6,72E-04	12,0 ± 1,5
10A	0,92 ± 0,104	No	-	4,95E+05 ± 2,20E+04	2,81E-02 ± 2,23E-03	56,8 ± 3,8
12A	1,32 ± 0,270	Yes	4,19 ± 0,29	2,64E+05 ± 6,11E+04	9,10E-04 ± 7,01E-05	3,6 ± 1,0
14A	16,41 ± 0,296 *	No	-	N.A.	N.A.	N.A.
15A	1,06 ± 0,157	No	-	4,71E+05 ± 7,05E+04	8,79E-03 ± 1,06E-03	18,7 ± 0,9
16A	3,75 ± 1,133	Yes	10,20 ± 2,59	1,87E+05 ± 3,13E+04	1,44E-03 ± 1,38E-04	7,9 ± 1,4
18A	0,50 ± 0,003	No	-	4,15E+05 ± 4,32E+04	1,44E-02 ± 6,14E-04	35,1 ± 5,4
25A	0,16 ± 0,055	Yes	0,40 ± 0,40	1,21E+05 ± 5,95E+04	2,99E-04 ± 1,09E-04	2,7 ± 0,8
26A	0,42 ± 0,217	No	-	5,11E+05 ± 1,07E+05	2,26E-02 ± 2,23E-03	45,7 ± 11,5
29A	1,80 ± 0,588	Yes	6,01 ± 1,95	2,76E+05 ± 3,00E+04	3,07E-03 ± 3,42E-05	11,2 ± 1,3
30A	0,25 ± 0,020	No	-	1,72E+05 ± 5,26E+04	6,23E-04 ± 2,60E-05	3,8 ± 1,0

Supplementary online material

Materials and Methods

Quality control tests report good purity and stability of generated antibodies

To assess the quality control (QC) from the generated antibodies the monomericity, purity and temperature stability was checked. Monomericity was checked in duplicate via SEC-UPLC. All candidates present more than 95% monomericity. F/T test had non-significant impact on protein characteristic as all candidates present the same monomericity after 10 F/T cycles, with a recovery around 100%. However, incubating samples at high temperature for one week drastically affects de quality of some of the candidates leading to aggregates formation, with a recovery range from 45 to 97%.

Purity was determined via CE-SDS. Under non-reducing conditions, the intact IgG purity shows some signs of fragmentation, although values are higher than 90%. Under reducing conditions, the total IgG content, sum of light chain and heavy chain purity, is above 95%.

In short, anti-mTNFR2 generated antibodies present good monomericity and purity output, and while all of them remain stable at freezing temperatures, high temperatures might affect the stability of some of them.

Modelling of mouse TNFR2 and TNFα complex

The human TNFR2 model, 74% similar to mouse TNFR2, was used to summarize the binding sites of generated anti-mTNFR2 antibodies. The crystal structure of hTNFR2-hTNFα trimer (PDB: 3ALQ), was uploaded into PyMol v2.3.3 (Schrondinger) software.

Supplementary Table 1. Antibody sequences. Sequences of constant and variable of heavy and light chains of novel generated rat anti-mTNFR2 IgG2a antibodies. Variable heavy (VH), constant heavy (CH), variable light (VL) and variable constant (CL).

Candidate 5A
Heavy chain protein sequence – Complete integrity
VH: EIQLVESGGGLVKPGTSLKLSCVASGFTFSDYWMTWVRQTPGKTMEWIGDIKND GSFTNYSPSLKNRFTISRDNAKSTLYLQMSNLRSEDTATYSCTTSPQWAYWGQGT LVTVSS CH: TETTAPSVYPLAPGTALKSNSMVTLGCLVKGYFPEPVTVTWNSGALSSGVHTFPA VLQSGLYTLTSSVTVPSSTWSSQAVTCNVAHPASSTKVDKKIVPRECNPCGCTGSE VSSVFIFPPKTKDVLTITLTPKVTCVVVDISQNDPEVRFSWFIDDVEVHTAQTHAPE KQSNSTLRSVSELPIVHRDWLNGKTFKCKVNSGAFPAPIEKSISKPEGTPRGPQVYT MAPPKEEMTQSQVSITCMVKGFYPPDIYTEWKMNGQPQENYKNTPPTMDTDGSY FLYSKLNVKKETWQQGNTFTCSVLHEGLHNHHTEKSLSHSPGK
Light chain protein sequence – type Kappa – Complete integrity
VL: DIQMTQSPSSLPASLGDRVTITCRASQDIGNFLRWFLQRPGKSPRLMIYGASNLAV GVPSRFSGSRSGSDYSLTISSLESEDMADYYCLQSKESPFTFGSGTKVEIK CL: RADAAPTVSIFPPSMEQLTSGGATVVCFVNNFYPRDISVKWKIDGSEQRDGVLDSV TDQDSKDSTYSMSSTLSLTKVEYERHNLYTCEVVHKTSSSPVVKSFNRNEC
Candidate 6A

Heavy chain protein sequence – Complete integrity
VH: EVQLVESGGGLVQPGRSLKLSCVASGFTFSNYGIHWFRQAPTKGLEWVASISPSGD TTYYRDSVKGRFTISRDNAKNTLYLQMDSLRSEDTATYYCATAPLSAYWGQGTL VTVSS CH: AETTAPSVYPLAPGTALKSNSMVTLGCLVKGYFPEPVTVTWNSGALSSGVHTFPA VLQSGLYTLTSSVTVPSSTWSSQAVTCNVAHPASSTKVDKKIVPRECNPCGCTGSE VSSVFIFPPKTKDVLTITLTPKVTCVVVDISQNDPEVRFSWFIDDVEVHTAQTHAPE KQSNSTLRSVSELPIVHRDWLNGKTFKCKVNSGAFPAPIEKSISKPEGTPRGPQVYT MAPPKEEMTQSQVSITCMVKGFYPPDIYTEWKMNGQPQENYKNTPPTMDTDGSY FLYSKLNVKKETWQQGNTFTCSVLHEGLHNHHTEKSLSHSPGK
Light chain protein sequence – type Kappa – Complete integrity
VL: DIQMTQSPSSMSASLGDRVTITCQASQDIGNNLIWFQQKPGKSPRPMIYYVTNLAK GVPSRFSGSRSGSDYSLTISSLESEDMADYHCLQYKQYPLAFGSGTKLEIK CL: RADAAPTVSIFPPSMEQLTSGGATVVCFVNNFYPRDISVKWKIDGSEQRDGVLDSV TDQDSKDSTYSMSSTLSLTKVEYERHNLYTCEVVHKTSSSPVVKSFNRNEC
Candidate 8A
Heavy chain protein sequence – Complete integrity
VH: EVQLQQSGPEVGRPGSSVKISCKASGYTFTDYFMNWLKQSPGQGLEWIGWIDPEY GSTDYAEKFKKKATLTADTSSSTAYIQLSSLTSEDTATYFCARGMYGTDYYYNNW FPCWGQGTLVTVSS

CH: AETTAPSVYPLAPGTALKSNSMVTLGCLVKGYFPEPVTVTWNSGALSSGVHTFPA VLQSGLYTLTSSVTVPSSTWSSQAVTCNVAHPASSTKVDKKIVPRECNPCGCTGSE VSSVFIFPPKTKDVLTITLTPKVTCVVVDISQNDPEVRFSWFIDDVEVHTAQTHAPE KQSNSTLRSVSELPIVHRDWLNGKTFKCKVNSGAFPAPIEKSISKPEGTPRGPQVYT MAPPKEEMTQSQVSITCMVKGFYPPDIYTEWKMNGQPQENYKNTPPTMDTDGSY FLYSKLNVKKETWQQGNTFTCSVLHEGLHNHHTEKSLSHSPGK
Light chain protein sequence – type Kappa – Complete integrity
VL: DIVMTQSPSSLAVSAGETVTLNCKSSQSLLSSGNQRNYLAWFHQKPGQSPKLLIYL ASTRESGVPDRFIGSGSGTDFTLTISTMQAEDLAVYFCQQHYDTPFTFGPGTKLELK CL: RADAAPTVSIFPPSMEQLTSGGATVVCFVNNFYPRDISVKWKIDGSEQRDGVLDSV TDQDSKDSTYSMSSTLSLTKVEYERHNLYTCEVVHKTSSSPVVKSFNRNEC
Candidate 10A
Heavy chain protein sequence – Complete integrity
VH: EVQLVETGGGLVRPGSSLKLSCATSGFTFSNTWMNWVRQAPGKGLEWVALIKDK YDNYEANYAESVKGRFTISRDDSKSRVYLQMNTLRVQDTATYYCTRQLNWFAY WGQGTLVTVSS CH: AETTAPSVYPLAPGTALKSNSMVTLGCLVKGYFPEPVTVTWNSGALSSGVHTFPA VLQSGLYTLTSSVTVPSSTWSSQAVTCNVAHPASSTKVDKKIVPRECNPCGCTGSE VSSVFIFPPKTKDVLTITLTPKVTCVVVDISQNDPEVRFSWFIDDVEVHTAQTHAPE KQSNSTLRSVSELPIVHRDWLNGKTFKCKVNSGAFPAPIEKSISKPEGTPRGPQVYT

MAPPKEEMTQSQVSITCMVKGFYPPDIYTEWKMNGQPQENYKNTPPTMDTDGSY FLYSKLNVKKETWQQGNTFTCSVLHEGLHNHHTEKSLSHSPGK
Light chain protein sequence – type Kappa – Complete integrity
VL: EIVLTQSPTTMTASPGEKVTITCRASSSVSYMHWYQQKPGASPKPWIYETSKLASG VPDRFSGSGSGTSYSLTINNMEAEDAATYYCQQWNYPWTFGGGTKLELK CL: RADAAPTVSIFPPSMEQLTSGGATVVCFVNNFYPRDISVKWKIDGSEQRDGVLDSV TDQDSKDSTYSMSSTLSLTKVEYERHNLYTCEVVHKTSSSPVVKSFNRNEC
Candidate 12A
Heavy chain protein sequence – Partial integrity
VH: EVQLVESGGGLVQPGKSLKLSCEASGFTFSDYHMAWVRQAPKKGLEWVATIVFD GSRTYYRDSVKGRFTISRYNSKSTLYLQMDSLRSEDTATYYCATQETGSSDYWGQ GVMVTVSS CH: AETTAPSVYPLAPGTALKSNSMVTLGCLVKGYFPEPVTVTWNSGALSSGVHTFPA VLQSGLYTLTSSVTVPSSTWSSQAVTCNVAHPASSTKVDKKIVPRECNPCGCTGSE VSSVFIFPPKTKDVLTITLTPKVTCVVVDISQNDPEVRFSWFIDDVEVHTAQTHAPE KQSNSTLRSVSELPIVHRDWLNGKTFKCKVNSGAFPAPIEKSISKPEGTPRGPQVYT MAPPKEEMTQSQVSITCMVKGFYPPDIYTEWKMNGQPQENYKNTPPTMDTDGSY FLYSKLNVKKETWQQGNTFTCSVLHERSEEHTSELQSPEAISYAVFCLKRGGGGG GG
Light chain protein sequence – type Kappa – Complete integrity

VL: DIQMTQSPSSLPASLGERVTISCRASQGISKKLNWYQQKPDGTINPLIYYTSNLQFG VPSRFSGSGSGTDYSLTLSSLEPEDFAMYYCQQDASFPPTFGGGTKLELK CL: RADAAPTVSIFPPSMEQLTSGGATVVCFVNNFYPRDISVKWKIDGSEQRDGVLDSV TDQDSKDSTYSMSSTLSLTKVEYERHNLYTCEVVHKTSSSPVVKSFNRNEC
Candidate 14A
Heavy chain protein sequence – Complete integrity
VH: EVQLQESGPGLVKPSQSLSLTCSVTGYSITSTYRWNWIRKFPGNKLEWMGYINSA GTTNYNPSLKSRISITRETSKNQFFLQVNSVTTEDTATYYCARDYDGYLNVYFDY WGQGVMVTVSS CH: AETTAPSVYPLAPGTALKSNSMVTLGCLVKGYFPEPVTVTWNSGALSSGVHTFPA VLQSGLYTLTSSVTVPSSTWSSQAVTCNVAHPASSTKVDKKIVPRECNPCGCTGSE VSSVFIFPPKTKDVLTITLTPKVTCVVVDISQNDPEVRFSWFIDDVEVHTAQTHAPE KQSNSTLRSVSELPIVHRDWLNGKTFKCKVNSGAFPAPIEKSISKPEGTPRGPQVYT MAPPKEEMTQSQVSITCMVKGFYPPDIYTEWKMNGQPQENYKNTPPTMDTDGSY FLYSKLNVKKETWQQGNTFTCSVLHEGLHNHHTEKSLSHSPGK
Light chain protein sequence – type lambda – Complete integrity
VL: QVVLTQPKSVSTSLESTVKLSCKLNSGNIGSYYMHWYQQHEGRSPTNMIYRDDKR PDGVPDRFSGSIDSSSNSAFLTINNVQTEDEAIYFCHSYDSSINIFGGGTKLTVLG CL:

QPKSTPTLTVFPPSTEELQGNKATLVCLISDFYPSDVEVAWKANGAPISQGVDTAN PTKQGNKYIASSFLRLTAEQWRSRNSFTCQVTHEGNTVEKSLSPAECV
Candidate 15A
Heavy chain protein sequence – Complete integrity
VH: EVQLVESGGGLVQPGSSLKLSCVVSGFTFSNYGMNWIRQAPKKGLEWIAMIYFDS SNKYYADSVKGRFTISRDNSKNTLYLEMNSLRSEDTAMYYCARYYYDGTYYDYF DYWGQGVMVTVSS CH: AETTAPSVYPLAPGTALKSNSMVTLGCLVKGYFPEPVTVTWNSGALSSGVHTFPA VLQSGLYTLTSSVTVPSSTWSSQAVTCNVAHPASSTKVDKKIVPRECNPCGCTGSE VSSVFIFPPKTKDVLTITLTPKVTCVVVDISQNDPEVRFSWFIDDVEVHTAQTHAPE KQSNSTLRSVSELPIVHRDWLNGKTFKCKVNSGAFPAPIEKSISKPEGTPRGPQVYT MAPPKEEMTQSQVSITCMVKGFYPPDIYTEWKMNGQPQENYKNTPPTMDTDGSY FLYSKLNVKKETWQQGNTFTCSVLHEGLHNHHTEKSLSHSPGK
Light chain protein sequence – type Kappa – Complete integrity
VL: EIVLTQSPTAMAASPGEKVTLICLASSSVTCMNWYQQKSGASPKLWIYGTSNLAS GVPNRFSGSGSGTSYSLTIISMEAEDVATYYCLQLSSYPPTWTFGGGTKLELK CL: RADAAPTVSIFPPSMEQLTSGGATVVCFVNNFYPRDISVKWKIDGSEQRDGVLDSV TDQDSKDSTYSMSSTLSLTKVEYERHNLYTCEVVHKTSSSPVVKSFNRNEC
Candidate 16A
Heavy chain protein sequence – Complete integrity

VH:

EVKLVESGGGLVQPGRSLKLSCVASGFTFNNYWMTWIRQAPGKGLEWVTSITNT

DGNTYYPDSVKGRFTVSRDNAKTTLYLQLNSLRSEDTATYYCTRGGDGTYYYGV

MDAWGQGASVTVSS

CH:

AETTAPSVYPLAPGTALKSNSMVTLGCLVKGYFPEPVTVTWNSGALSSGVHTFPA

VLQSGLYTLTSSVTVPSSTWSSQAVTCNVAHPASSTKVDKKIVPRECNPCGCTGSE

VSSVFIFPPKTKDVLTITLTPKVTCVVVDISQNDPEVRFSWFIDDVEVHTAQTHAPE

KQSNSTLRSVSELPIVHRDWLNGKTFKCKVNSGAFPAPIEKSISKPEGTPRGPQVYT

MAPPKEEMTQSQVSITCMVKGFYPPDIYTEWKMNGQPQENYKNTPPTMDTDGSY

FLYSKLNVKKETWQQGNTFTCSVLHEGLHNHHTEKSLSHSPGK

Light chain protein sequence – type Kappa – Complete integrity

VL:

NIQLTQSPSLLSASVGDRVTLSCKGSQNINNYLAWYQQKLGEAPKLLIYNTNSLQT

GFPSRFSGSGSGTDYTLTITSLQPEDVATYFCYEYNNGYAFGPGTKLELK

CL:

RADAAPTVSIFPPSMEQLTSGGATVVCFVNNFYPRDISVKWKIDGSEQRDGVLDSV

TDQDSKDSTYSMSSTLSLTKVEYERHNLYTCEVVHKTSSSPVVKSFNRNEC

Candidate 18A

Heavy chain protein sequence – Complete integrity

VH:

EVQLVESGGGLVQPGRSLKLSCAASGFTFSNFGMHWIRQAPTKGLEWVASISPSG

GNTYYRDSVKGRLTISRDNAKSTLYLQLDSLRSEDTATYYCARGETTGIQDWFAY

WGQGTLVTVSS

CH:

AETTAPSVYPLAPGTALKSNSMVTLGCLVKGYFPEPVTVTWNSGALSSGVHTFPA VLQSGLYTLTSSVTVPSSTWSSQAVTCNVAHPASSTKVDKKIVPRECNPCGCTGSE VSSVFIFPPKTKDVLTITLTPKVTCVVVDISQNDPEVRFSWFIDDVEVHTAQTHAPE KQSNSTLRSVSELPIVHRDWLNGKTFKCKVNSGAFPAPIEKSISKPEGTPRGPQVYT MAPPKEEMTQSQVSITCMVKGFYPPDIYTEWKMNGQPQENYKNTPPTMDTDGSY FLYSKLNVKKETWQQGNTFTCSVLHEGLHNHHTEKSLSHSPGK
Light chain protein sequence – type Kappa – Complete integrity
VL: DIQMTQSPSFLSASVGERVTLSCRASQNINRYLDWYQQKLGETPKLLMYNTINLHT GIPSRFSGSGSGTDYTLTISSLQPEDVATYFCLQRNSWPNTFGAGTKLELK CL: RADAAPTVSIFPPSMEQLTSGGATVVCFVNNFYPRDISVKWKIDGSEQRDGVLDSV TDQDSKDSTYSMSSTLSLTKVEYERHNLYTCEVVHKTSSSPVVKSFNRNEC
Candidate 25A
Heavy chain protein sequence – Complete integrity
VH: EVQLVESGGGLVQPGRSLKVSCTVSGFTFSDYDMAWVRQTPMKGLEWVASISTG GGNTYYRDSVKGRFTISRDNAKNIQYLQMDSLRSEDTATYYCATNYGGYSESDFF DYWGQGVMVTVSS CH: AETTAPSVYPLAPGTALKSNSMVTLGCLVKGYFPEPVTVTWNSGALSSGVHTFPA VLQSGLYTLTSSVTVPSSTWSSQAVTCNVAHPASSTKVDKKIVPRECNPCGCTGSE VSSVFIFPPKTKDVLTITLTPKVTCVVVDISQNDPEVRFSWFIDDVEVHTAQTHAPE KQSNSTLRSVSELPIVHRDWLNGKTFKCKVNSGAFPAPIEKSISKPEGTPRGPQVYT

MAPPKEEMTQSQVSITCMVKGFYPPDIYTEWKMNGQPQENYKNTPPTMDTDGSY FLYSKLNVKKETWQQGNTFTCSVLHEGLHNHHTEKSLSHSPGK
Light chain protein sequence – type Kappa – Complete integrity
VL: DIQMTQSPSSLPSSLGERVTISCRASQGISNNLNWYQQKPDGTIKPLIYYTSNLQSG VPSRFSGSGSGTDYSLTISSLEPEDFAMYYCQQDAIFPNTFGAGTKLELK CL: RADAAPTVSIFPPSMEQLTSGGATVVCFVNNFYPRDISVKWKIDGSEQRDGVLDSV TDQDSKDSTYSMSSTLSLTKVEYERHNLYTCEVVHKTSSSPVVKSFNRNEC
Candidate 26A
Heavy chain protein sequence – Complete integrity
VH: EVQLVETGGGLVRPGSSLKLSCVTSGFTFSNTWMNWVRQAPGKGLEWVALIKDK YDNYEANYAESVKGRFTISRDDSKSRVYLQMNTLRDQDTATYYCTRQLNWFAY WGQGTLVTVSS CH: AETTAPSVYPLAPGTALKSNSMVTLGCLVKGYFPEPVTVTWNSGALSSGVHTFPA VLQSGLYTLTSSVTVPSSTWSSQAVTCNVAHPASSTKVDKKIVPRECNPCGCTGSE VSSVFIFPPKTKDVLTITLTPKVTCVVVDISQNDPEVRFSWFIDDVEVHTAQTHAPE KQSNSTLRSVSELPIVHRDWLNGKTFKCKVNSGAFPAPIEKSISKPEGTPRGPQVYT MAPPKEEMTQSQVSITCMVKGFYPPDIYTEWKMNGQPQENYKNTPPTMDTDGSY FLYSKLNVKKETWQQGNTFTCSVLHEGLHNHHTEKSLSHSPGK
Light chain protein sequence – type Kappa – Complete integrity
VL:

EIVLTQSPTTMTASPGEKVTITCRASTSVSYMHWYQQKAGASPKPWIYETSKLASG VPDRFSGSGSGTSYSLTINNMEAEDAATYYCQQWNYPWTFGGGTKLELK CL: RADAAPTVSIFPPSMEQLTSGGATVVCFVNNFYPRDISVKWKIDGSEQRDGVLDSV TDQDSKDSTYSMSSTLSLTKVEYERHNLYTCEVVHKTSSSPVVKSFNRNEC
Candidate 29A
Heavy chain protein sequence – Complete integrity
VH: EVQLVESGGGLEQPGRSLKLSCVASGFTFSDYHMAWVRQAPKKGLEWVATIIYD GSRTYYRDSVKGRFTISRDNAKSTLYLQMDSLRSEDTATYYCATQGTGSSDYWG QGVMVTVSS CH: AETTAPSVYPLAPGTALKSNSMVTLGCLVKGYFPEPVTVTWNSGALSSGVHTFPA VLQSGLYTLTSSVTVPSSTWSSQAVTCNVAHPASSTKVDKKIVPRECNPCGCTGSE VSSVFIFPPKTKDVLTITLTPKVTCVVVDISQNDPEVRFSWFIDDVEVHTAQTHAPE KQSNSTLRSVSELPIVHRDWLNGKTFKCKVNSGAFPAPIEKSISKPEGTPRGPQVYT MAPPKEEMTQSQVSITCMVKGFYPPDIYTEWKMNGQPQENYKNTPPTMDTDGSY FLYSKLNVKKETWQQGNTFTCSVLHEGLHNHHTEKSLSHSPGK
Light chain protein sequence – N.A.
Candidate 30A
Heavy chain protein sequence – Complete integrity
VH:

EVQLVETGGGLVRPGSSLKLSCATSGFTFSNTWMNWVRQAPGKGLEWVALVKD EYNDYEANYAESVKGRFTISRDDSKSRVYLQMNTLRDQDTATYYCTRTAYYGLF PYWGQGSLVTVSS CH: AETTAPSVYPLAPGTALKSNSMVTLGCLVKGYFPEPVTVTWNSGALSSGVHTFPA VLQSGLYTLTSSVTVPSSTWSSQAVTCNVAHPASSTKVDKKIVPRECNPCGCTGSE VSSVFIFPPKTKDVLTITLTPKVTCVVVDISQNDPEVRFSWFIDDVEVHTAQTHAPE KQSNSTLRSVSELPIVHRDWLNGKTFKCKVNSGAFPAPIEKSISKPEGTPRGPQVYT MAPPKEEMTQSQVSITCMVKGFYPPDIYTEWKMNGQPQENYKNTPPTMDTDGSY FLYSKLNVKKETWQQGNTFTCSVLHEGLHNHHTEKSLSHSPGK
Light chain protein sequence – Incomplete integrity
VL: DIQMTQSPASLSSSLGETVTIECRASEDIYSNLAWYQQKPGNSPQLLIFDANTLADG VPSRFSGSGSGPQYSLHINSLQSEDVASYFCQQYNNYPLTFGSGTRLEIK CL: RADAAPTVSIFPPSMEQLTSGGATVVCFVNNFYPRDISVKWKIDGSEQRDGVLDSV TDQDSKDSTYSMSSTLSLTKVEYERHNLYTCEVVHKTSSSPVVKSFNRNEC

754

Supplementary Table 2. Overall quality control for monomericity and purity of anti-mTNFR2 mAbs purified. Monomericity data represented as mean and SD of antibodies produced of two independent experiments (n=2). Monomericity was checked to test the temperature stability: after 10 cycles of freeze-and-thaw (F/T) and after 1 week incubation at 40 °C in a single independent experiment . Purity was assessed via CE-SDS non-reduced (NR) and reduced (R).

			Stability test		NR CE-SDS	R CE-SDS
Anti-TNFR2 mAbs	**Concentration (mg/ml)**	**Monomer average (% ± SD)**	**Monomer (%) *post 10 cycles F/T***	**Monomer (%) post 1 week incubation 40 °C**	**Intact IgG (%)**	**LC+HC (%)**
5A	2,08	98,80 ± 0,14	99,70	67,90	90,90	98,40
6A	1,18	95,64 ± 0,20	96,10	92,50	N.A.	97,70
8A	0,77	95,30 ± 0,14	95,70	85,20	95,10	98,60
10A	1,47	98,70 ± 0,14	98,90	89,70	90,50	99,60
12A	0,99	99,02 ± 0,16	99,20	72,00	93,00	99,50
14A	1,53	98,81 ± 0,30	98,90	71,50	91,00	99,40
15A	1,16	99,12 ± 0,54	99,50	64,00	93,50	98,70
16A	1,52	99,18 ± 0,03	99,40	45,20	93,80	98,70
18A	2,31	98,69 ± 0,40	98,70	93,80	92,10	99,40
25A	2,16	99,13 ± 0,18	99,10	78,30	93,20	99,10
26A	2,12	98,55 ± 0,21	98,70	89,40	92,40	99,20
29A	1,76	98,32 ± 0,17	98,10	71,80	91,60	99,10
30A	1,80	99,52 ± 0,31	99,50	85,50	90,60	99,20

762 **Sup. Table 3.** Treg staining percentages and MFI. Percentage of TNFR2- and TNFR2+ Tregs
763 stained either with hamster-anti-TNFR2 PE antibody (clone TR75-89), rat-anti-TNFR2
764 antibody or both. gMFI for TNFR2 signal detected by AF647 signal. Data representative of
765 single experiment out of two independent experiments.

Abs	% Tregs TNFR2-	% Tregs TNFR2+ (PE+)	% Tregs TNFR2+ (PE+ and AF647+)	% Tregs TNFR2+ (AF647+)	gMFI AF647 signal in CD3+ YFP+
5A	61,45	33,10	2,68	2,77	442
6A	73,15	0,11	3,80	22,95	1118
8A	66,90	0,11	1,97	31,05	1267
10A	71,25	10,15	6,40	12,21	401
12A	53,95	1,63	23,55	20,88	1344
14A	70,95	1,93	18,15	8,97	1019
15A	64,25	0,50	13,30	21,98	1169
16A	55,35	0,97	23,90	19,78	1504
18A	63,15	30,45	4,50	1,90	471
25A	52,75	0,90	21,25	25,16	1466
26A	66,55	19,97	10,35	3,16	485
29A	62,95	2,39	21,45	13,22	1357
30A	48,05	0,06	17,65	34,15	1154
rat isotype	56,00	32,95	3,45	2,64	346

766

767

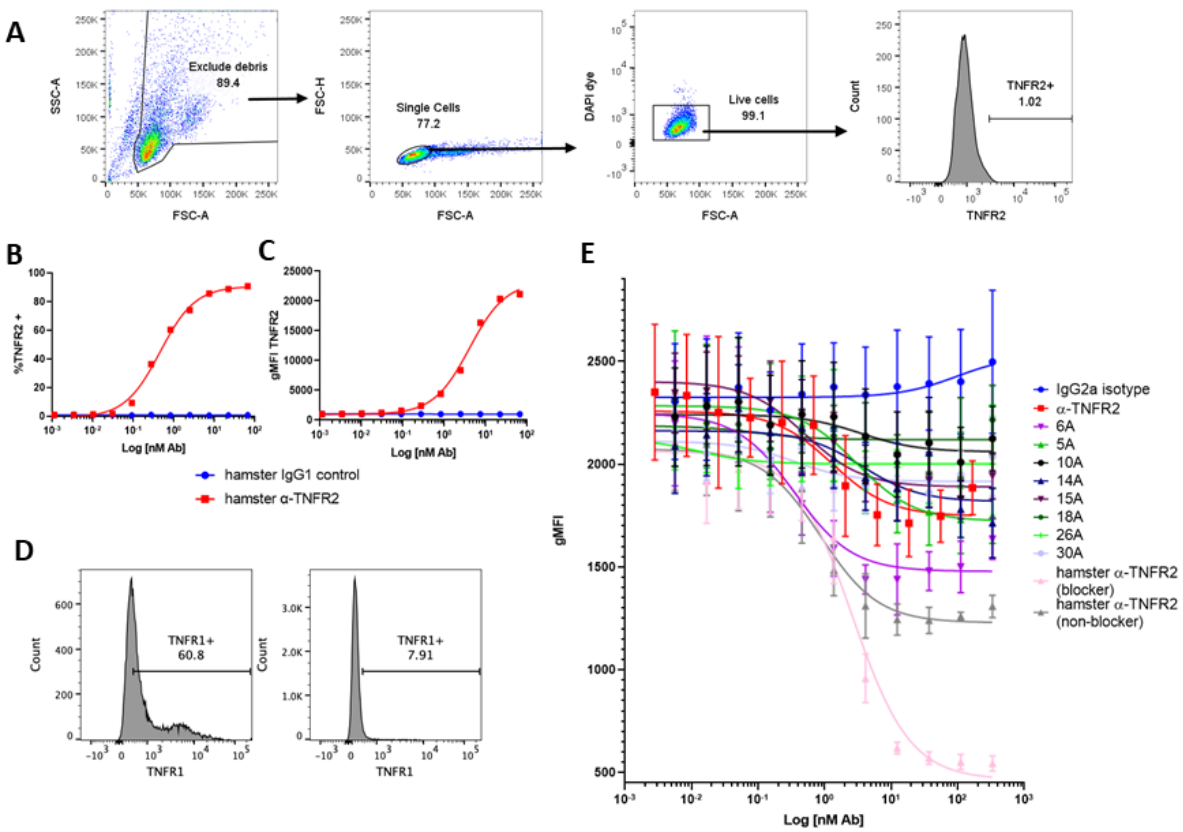

Figure S1. Characterization of anti-mouse TNFR2 antibodies in vitro. (A) Gating strategy followed. Gating was done on unstained CHO-K1.mTNFR2 cells. First, cell debris was excluded based on FSC-A / SSC-A properties. Next, single cells were gated based on FSC-A / FSC-H. Live cells were gated based on FSC-A / DAPI properties. Next to the live unstained single cell population, a mouseTNFR2+ gate was set based on TNFR2 histogram. Data representative of single experiment out of three independent experiments. (B and C) mTNFR2 expression was checked in stable transfected CHO-K1 cells which were incubated with 3-fold increasing concentrations of each rat IgG2a mAb TNFR2 expression in stable transfected CHO-K1 via direct staining. Expression levels was detected by flow cytometry assessing TNFR2 + population percentage (B) and gMFI (C). Data representative of single experiment out of three independent experiments. (D) TNFR1 expression was tested on parental CHO-K1 (right) and transiently transfected CHO-K1 cells (left). TNFR1 gating was done on unstained CHO-K1 cells, similar as shown in (A). (E) TNF competition FACS of antibodies. Data represented as a three-parameter gMFI dose-response curve fit based on mean and SEM of

three independent experiments of the non-blocker antibodies with appropriate controls incubations with 3-fold increasing concentrations. Two benchmark hamster-anti-mTNFR2 antibodies with known blocking activity were added as controls.

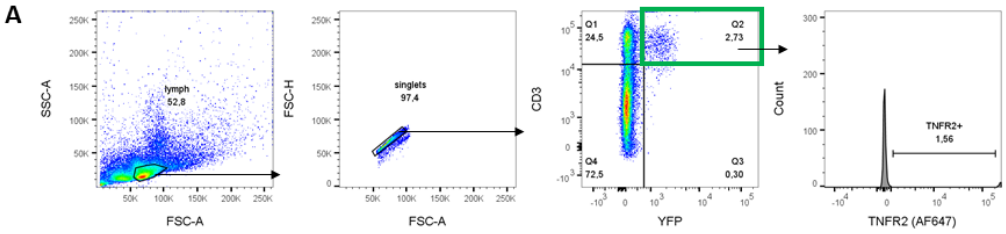

788

789 **Figure S2.** Characterization of anti-mouse TNFR2 antibodies with ex vivo material. (A) Treg
790 gating strategy followed. Gating was done on unstained freshly isolated splenocytes. First,
791 lymphocytes were gated based on FSC-A / SSC-A properties. Next, single cells were gated
792 based FSC-A / FSC-H. Treg population were gated as CD3 positive and FoxP3-YFP positive.
793 Next to the Treg population, a mouse TNFR2+ gate was set with a rat isotype control via
794 histogram. Data representative of single experiment out of two independent experiments.

795

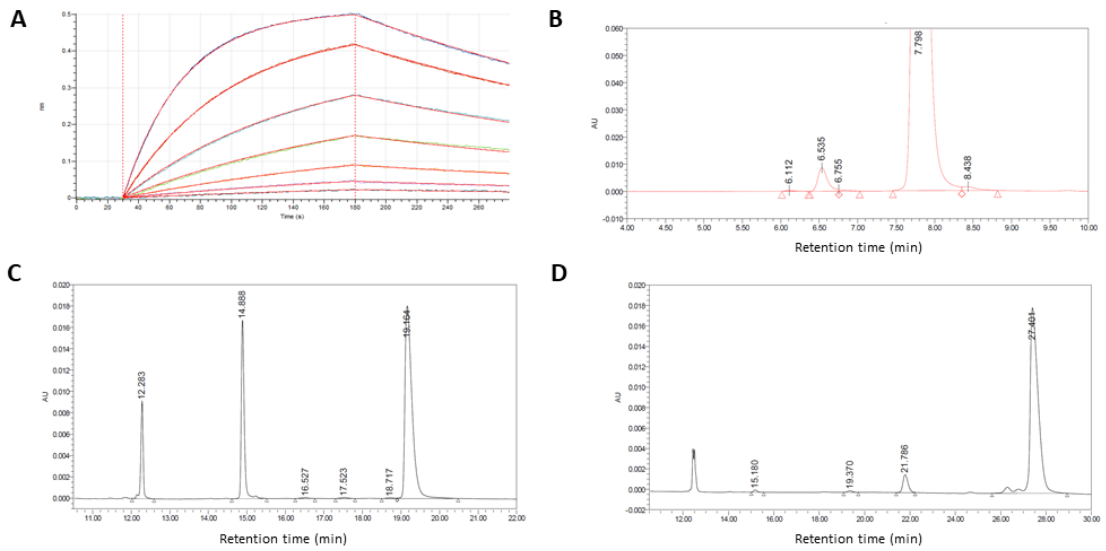

796

797 **Figure S3.** BLI representation, CE-SDS and SEC-HPLC. (A) BLI analysis of candidate for
798 binding to recombinant mTNFR2. The mAb association at 10 μg/ml to recombinant mTNFR2
799 protein loaded biosensors is displayed with 5-fold decreasing concentrations starting at 95 nM.
800 Data representative of three independent experiments. (B) Auto-scaled SEC-HPLC profile of
801 anti-mTNFR2 antibody. (C and D) Purity of mAb evaluated by CE-SDS. 10 kDa standard
802 marker (~12.3 mins) was used for the calibration of retention time for each trace, reduced (C)
803 and non-reduced (D). Numbers represent the retention time. Data representative of a single
804 mAb anti-mTNFR2, candidate 29; (B, C and D) data representative of a single independent
805 experiment.

806

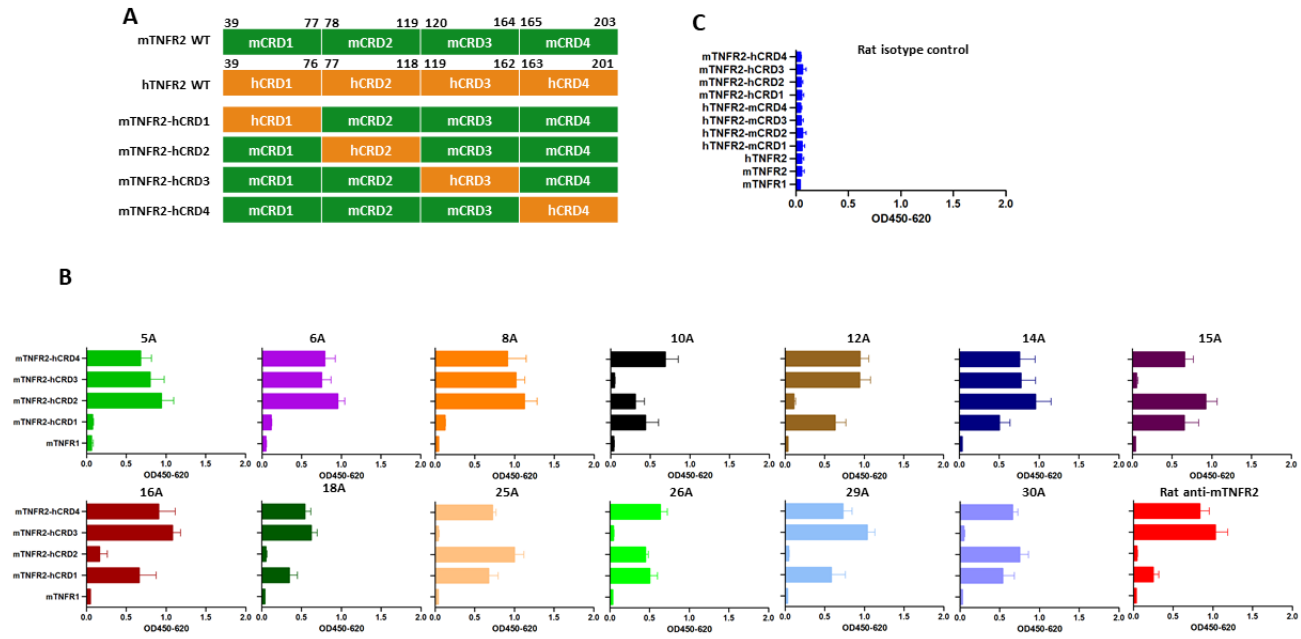

807

808 **Figure S4.** Characterization of anti-mTNFR2 mAbs targeting CRDs 1-4. (A) Schematic
809 representation of the 6 mouse-human TNF2 chimeras CRD1-CRD4 (Cystein Rich Domain).
810 (B) The targeting CRD of each mAb were determined by cell ELISA with mouse-human
811 TNFR2 domain swap mutants. mTNFR1 and CHO-empty vector targeting was included too.
812 (C) Targeting of rat isotype control included in all assays. All data represented as a three-
813 parameter OD450-620 detection based on mean and SD of three independent experiments.

814